Edge states and topological phases in non-Hermitian systems

Kenta Esaki,[1] Masatoshi Sato,[1] Kazuki Hasebe,[2] and Mahito Kohmoto[1]
[1]*Institute for Solid State Physics, University of Tokyo, Kashiwanoha 5-1-5, Kashiwa, Chiba 277-8581, Japan*
[2]*Department of General Education, Kagawa National College of Technology, Mitoyo, Kagawa 769-1192, Japan*
(Received 20 July 2011; published 17 November 2011)

Topological stability of the edge states is investigated for non-Hermitian systems. We examine two classes of non-Hermitian Hamiltonians supporting real bulk eigenenergies in weak non-Hermiticity: SU(1,1) and SO(3,2) Hamiltonians. As an SU(1,1) Hamiltonian, the tight-binding model on the honeycomb lattice with imaginary onsite potentials is examined. Edge states with $\mathrm{Re}E = 0$ and their topological stability are discussed by the winding number and the index theorem based on the pseudo-anti-Hermiticity of the system. As a higher-symmetric generalization of SU(1,1) Hamiltonians, we also consider SO(3,2) models. We investigate non-Hermitian generalization of the Luttinger Hamiltonian on the square lattice and that of the Kane-Mele model on the honeycomb lattice, respectively. Using the generalized Kramers theorem for the time-reversal operator Θ with $\Theta^2 = +1$ [M. Sato *et al.*, e-print arXiv:1106.1806], we introduce a time-reversal-invariant Chern number from which topological stability of gapless edge modes is argued.

DOI: 10.1103/PhysRevB.84.205128 PACS number(s): 73.43.Nq, 73.20.−r, 72.25.−b

I. INTRODUCTION

Recent developments of topological insulators have led to much interest in topological phases of matter. Murakami, Nagaosa, and Zhang predicted spin-Hall effect[1,2] by reexamining Hamiltonians describing hole-doped semiconductors with spin-orbit coupling presented by Luttinger (the Luttinger Hamiltonian).[3] After the theoretical predictions and experimental observations,[4,5] the spin-Hall effects were generalized to insulating systems.[6] Subsequently, the quantum version of the spin-Hall effect, the quantum spin-Hall effect, was introduced by Kane and Mele as a model with time-reversal symmetry in graphene[7] and independently by Bernevig and Zhang as two-dimensional (2D) semiconductor systems with a uniform strain gradient.[8] Remarkably, quantum spin-Hall effects were experimentally observed in 2D CdTe/HgTe/CdTe quantum well by König *et al.*,[9] following the theoretical predictions by Bernevig, Hughes, and Zhang.[10]

The appearance of the topologically protected gapless edge states within the bulk gap is a manifestation of the topological insulator. The number of such gapless edge modes is specified by topological invariants. In Ref. 11, gapless edge states carrying spin currents were found when the spin is conserved. They are characterized by spin Chern numbers introduced by Sheng *et al.*[12] The spin Chern number is an extension of the Chern number for quantized Hall conductivity[13,14] to quantized spin-Hall conductivity in time-reversal-symmetric systems with spin conservation. Kane and Mele introduced Z_2 invariants that distinguish topologically nontrivial phases from trivial ones in time-reversal-symmetric systems[7,15] even when the spin is not conserved. The above-mentioned gapless edge states in the quantum spin-Hall insulator, dubbed as the helical edge modes,[16] are known as a consequence of the Kramers theorem of the time-reversal symmetry Θ with $\Theta^2 = -1$. In contrast, time-reversal-symmetric systems with $\Theta^2 = +1$ have not been investigated so far in the context of topological insulators since they are considered to be irrelevant to topologically protected gapless edge states.

Recently, the present authors have shown that the (generalized) Kramers theorem follows even for $\Theta^2 = +1$ in a class of non-Hermitian systems (provided the metric operator is anticommutative with the time-reversal operator).[17] Therefore, a natural question arises: Do topologically protected edge modes also appear in such non-Hermitian models? The main purpose of this work is to give an answer to the question. We demonstrate numerical calculations and provide topological arguments for the stability of edge modes in non-Hermitian Hamiltonians. In particular, we investigate lattice versions of the SU(1,1) and SO(3,2) Hamiltonians studied in Ref. 17. (See, also, the related works in higher-dimensional quantum Hall effect[18,19] and in *PT*-symmetric quantum mechanics[20–22]). As a lattice realization of the SU(1,1) model, we consider the tight-binding model on the honeycomb lattice with imaginary onsite potentials. For the SO(3,2) model, we investigate non-Hermitian generalization of the Luttinger Hamiltonian[6,11] on the square lattice. We also argue a non-Hermitian generalization of the Kane-Mele model,[7,15] where the hopping integrals are asymmetric due to non-Hermiticity.

Non-Hermitian systems play important roles in physics. For instance, a non-Hermitian system with disorder, known as the Hatano-Nelson model, has been studied in the context of localization-delocalization transition in one and two dimensions.[23–25] The model simulates the depinning of flux lines in type-II superconductors subject to a transverse magnetic field.[23] We also briefly discuss possible relevance to the model.

The paper is organized as follows. In Sec. II, we introduce the SU(1,1) and SO(3,2) Hamiltonians and their basic structures. In Sec. III, a lattice version of the SU(1,1) model on graphene is explored, and the stability of edge states is discussed on the basis of topological arguments. We further investigate the SO(3,2) model on the square lattice in Sec. IV. A topological number for the non-Hermitian system is introduced in order to account for the stability of edge modes under small non-Hermitian perturbation. In Sec. V, a non-Hermitian version of the Kane-Mele model is presented and the topological property of the model is also discussed. Section VI is devoted to summary and discussions.

II. SU(1,1) AND SO(3,2) HAMILTONIANS

In this paper, we mainly consider SU(1,1) and SO(3,2) models, which are non-Hermitian generalizations of SU(2) and SO(5) models, respectively. Here, we briefly discuss their structures with emphasis on the relations to split quaternions along Ref. 17.

It is well known that the quaternion algebra is realized as 2×2 unit matrix 1_2 and (i times) Pauli matrices $i\sigma_a$ ($a = 1,2,3$). The SU(2) Hamiltonian is constructed by the Pauli matrices σ_a:

$$H = d_1\sigma_1 + d_2\sigma_2 + d_3\sigma_3, \tag{1}$$

where d_a ($a = 1,2,3$) are real. The eigenenergies are

$$E_\pm = \pm\sqrt{d_1^2 + d_2^2 + d_3^2}. \tag{2}$$

Similarly, the split quaternion algebra is realized as the 2×2 unit matrix 1_2 and (i times) SU(1,1) Pauli matrices ($-\sigma_1$, $-\sigma_2$,$i\sigma_3$), and the SU(1,1) Hamiltonian is constructed by such SU(1,1) Pauli matrices:

$$H = d_1\sigma_1 + d_2\sigma_2 + id_3\sigma_3. \tag{3}$$

The eigenenergies are

$$E_\pm = \pm\sqrt{d_1^2 + d_2^2 - d_3^2}. \tag{4}$$

The SO(5) gamma matrices Γ_a ($a = 1,2,\ldots,5$), are defined so as to satisfy the Clifford algebra $\{\Gamma_a,\Gamma_b\} = 2\delta_{ab}$. They have the quaternionic structure since their off-diagonal components are given by the "quaternions"

$$\Gamma_1 = \begin{pmatrix} 0 & i\sigma_1 \\ -i\sigma_1 & 0 \end{pmatrix}, \quad \Gamma_2 = \begin{pmatrix} 0 & i\sigma_2 \\ -i\sigma_2 & 0 \end{pmatrix},$$
$$\Gamma_3 = \begin{pmatrix} 0 & i\sigma_3 \\ -i\sigma_3 & 0 \end{pmatrix}, \quad \Gamma_4 = \begin{pmatrix} 0 & 1_2 \\ 1_2 & 0 \end{pmatrix}, \tag{5}$$
$$\Gamma_5 = \begin{pmatrix} 1_2 & 0 \\ 0 & -1_2 \end{pmatrix}.$$

With the SO(5) gamma matrices, the SO(5) Hamiltonian is given by

$$H = d_1\Gamma_1 + d_2\Gamma_2 + d_3\Gamma_3 + d_4\Gamma_4 + d_5\Gamma_5, \tag{6}$$

where d_a ($a = 1,2,\ldots,5$) are real. The eigenenergies are

$$E_\pm = \pm\sqrt{d_1^2 + d_2^2 + d_3^2 + d_4^2 + d_5^2}, \tag{7}$$

each of which is doubly degenerate. Such double degeneracy is understood as a consequence of the Kramers theorem since the SO(5) Hamiltonian is invariant under time-reversal operation $\Theta_-^2 = -1$ with

$$\Theta_- = \begin{pmatrix} i\sigma_2 & 0 \\ 0 & i\sigma_2 \end{pmatrix} \cdot K, \tag{8}$$

where K denotes the complex-conjugation operator. Similarly, the SO(3,2) gamma matrices are introduced as the matrices, the off-diagonal blocks of which are given by the split quaternions. Hence, the SO(3,2) gamma matrices are given by

$$\begin{pmatrix} 0 & -\sigma_1 \\ \sigma_1 & 0 \end{pmatrix}, \quad \begin{pmatrix} 0 & -\sigma_2 \\ \sigma_2 & 0 \end{pmatrix},$$
$$\begin{pmatrix} 0 & i\sigma_3 \\ -i\sigma_3 & 0 \end{pmatrix}, \quad \begin{pmatrix} 0 & 1_2 \\ 1_2 & 0 \end{pmatrix}, \quad \begin{pmatrix} 1_2 & 0 \\ 0 & -1_2 \end{pmatrix}, \tag{9}$$

which are $i\Gamma_1$, $i\Gamma_2$, Γ_3, Γ_4, Γ_5 with the SO(5) gamma matrices (5). From the SO(3,2) gamma matrices, we construct the SO(3,2) Hamiltonian as

$$H = id_1\Gamma_1 + id_2\Gamma_2 + d_3\Gamma_3 + d_4\Gamma_4 + d_5\Gamma_5. \tag{10}$$

The eigenenergies are

$$E_\pm = \pm\sqrt{d_3^2 + d_4^2 + d_5^2 - d_1^2 - d_2^2}, \tag{11}$$

each of which is doubly degenerate. The SO(3,2) Hamiltonian is invariant under time-reversal operation $\Theta_+^2 = +1$ with

$$\Theta_+ = \begin{pmatrix} \sigma_1 & 0 \\ 0 & \sigma_1 \end{pmatrix} \cdot K. \tag{12}$$

As discussed in Ref. 17, such double degeneracy is a consequence of the generalized Kramers theorem for $\Theta_+^2 = +1$. The metric operator that satisfies $\eta H \eta^{-1} = H^\dagger$ is given by

$$\eta = \begin{pmatrix} \sigma_3 & 0 \\ 0 & \sigma_3 \end{pmatrix}. \tag{13}$$

Apparently, η is anticommutative with Θ_+: $\{\eta,\Theta_+\} = 0$.

III. SU(1,1) MODEL AND WINDING NUMBERS

In this section, we investigate topological stability of the edge states of the SU(1,1) model. As an example, the tight-binding model on the honeycomb lattice with imaginary onsite potentials is considered. Such a honeycomb lattice could be realized as a cold-atomic system in an optical lattice.[26] It will be found that edge states with $\mathrm{Re}E = 0$ are robust under weak non-Hermiticity. We will also argue that their topological stability is guaranteed by topological reasoning.

The SU(1,1) Hamiltonian has been utilized to describe a decaying Rabi oscillation in quantum optics.[27] More recently, a similar Hamiltonian was studied in a context of a quantum walk on a bipartite one-dimensional lattice with imaginary potentials from a different topological point of view.[28] The results were applied to nuclear spin pumping.[29]

A. Graphene with imaginary sublattice potential

As a model with the SU(1,1) Hamiltonian, we consider the following tight-binding model on the honeycomb lattice:

$$H = t\sum_{\langle i,j\rangle}(c_i^\dagger c_j + \mathrm{H.c.}) - i\sum_i \lambda_i c_i^\dagger c_i \quad (\lambda_i > 0). \tag{14}$$

The first term is the nearest-neighbor hopping. The second term represents imaginary onsite sublattice potentials, which make the system non-Hermitian. Here, $\lambda_i = \lambda_a$ and λ_b for closed

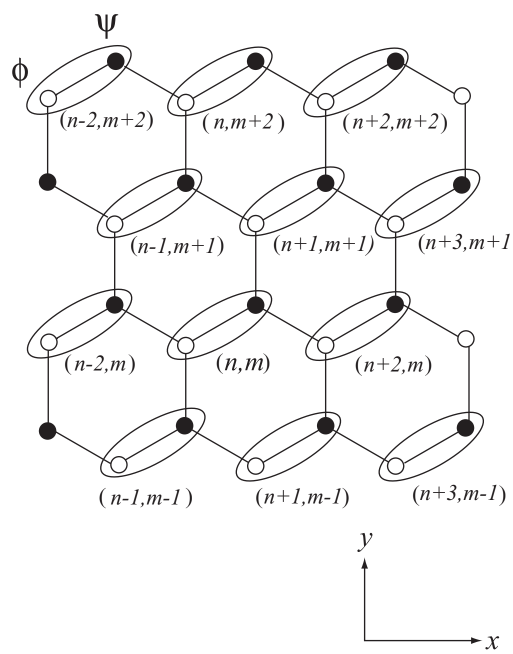

FIG. 1. The honeycomb lattice.

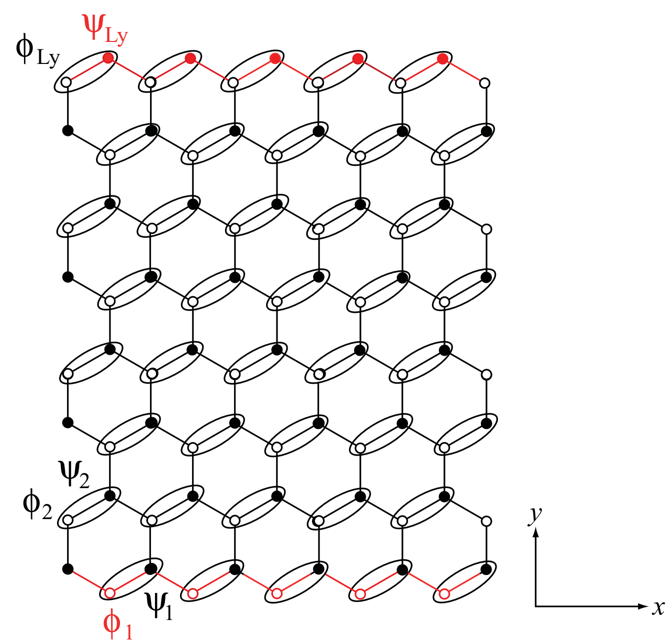

FIG. 2. (Color online) The honeycomb lattice with zigzag edges at $m = 1$ and 8 ($L_y = 8$) along the x direction.

and open circles in Fig. 1, respectively. The Hamiltonian (14) is rewritten as

$$H = t\sum_{\langle i,j\rangle}(c_i^\dagger c_j + \text{H.c.}) + i\lambda_V\sum_i \xi_i c_i^\dagger c_i - i\frac{\lambda_a+\lambda_b}{2}\sum_i c_i^\dagger c_i, \tag{15}$$

where $\lambda_V = \frac{\lambda_b-\lambda_a}{2}$ and $\xi_i = +1\ (-1)$ for closed (open) circles in Fig. 1. Since the $-i\frac{\lambda_a+\lambda_b}{2}\sum_i c_i^\dagger c_i$ term only shifts the origin of the energy, we neglect it in the following:

$$H = t\sum_{\langle i,j\rangle}(c_i^\dagger c_j + \text{H.c.}) + i\lambda_V\sum_i \xi_i c_i^\dagger c_i. \tag{16}$$

In the absence of edges, Eq. (16) reduces to the following SU(1,1) Hamiltonian in the momentum space:

$$H(\boldsymbol{k}) = \begin{pmatrix} i\lambda_V & 2t\cos\left(\frac{k_x a}{2}\right) + te^{i\frac{\sqrt{3}k_y a}{2}} \\ 2t\cos\left(\frac{k_x a}{2}\right) + te^{-i\frac{\sqrt{3}k_y a}{2}} & -i\lambda_V \end{pmatrix}, \tag{17}$$

which is obtained by the Fourier transformations

$$\begin{aligned} c_i &= \psi_{(n,m)} = \sum_{\boldsymbol{k}} e^{i\frac{a}{2}k_x n + i\frac{\sqrt{3}a}{2}k_y m}\psi_{\boldsymbol{k}}, \\ c_{i+\boldsymbol{d}} &= \phi_{(n+1,m+1)} = \sum_{\boldsymbol{k}} e^{i\frac{a}{2}k_x n + i\frac{\sqrt{3}a}{2}k_y(m+1)}\phi_{\boldsymbol{k}}. \end{aligned} \tag{18}$$

Here, $\psi_{\boldsymbol{k}}$ and $\phi_{\boldsymbol{k}}$ are the annihilation operators in the momentum space corresponding to the closed and the open circles in Fig. 1, respectively, k_x (k_y) is the momentum in the x (y) direction, a is the lattice constant of the honeycomb lattice, and $\boldsymbol{d} = a\hat{\boldsymbol{y}}/\sqrt{3}$. The bulk spectra of the system are obtained by diagonalizing the Hamiltonian (17) as

$$E_\pm(\boldsymbol{k}) = \pm\sqrt{\left|t + 2t\cos\left(\frac{k_x a}{2}\right)e^{i\frac{\sqrt{3}k_y a}{2}}\right|^2 - \lambda_V^2}. \tag{19}$$

Let us now examine the edge state in this system. If we make zigzag edges along the x direction as shown in Fig. 2, a zero-energy edge band appears in addition to the bulk bands (19). For the Hermitian case $\lambda_V = 0$, it has been known that the edge state with $E = 0$ appears for $2\pi/3 < ak_x < 4\pi/3$ as shown in Fig. 3.[30] We find here that the zero-energy edge state persists even in the presence of weak non-Hermiticity λ_V

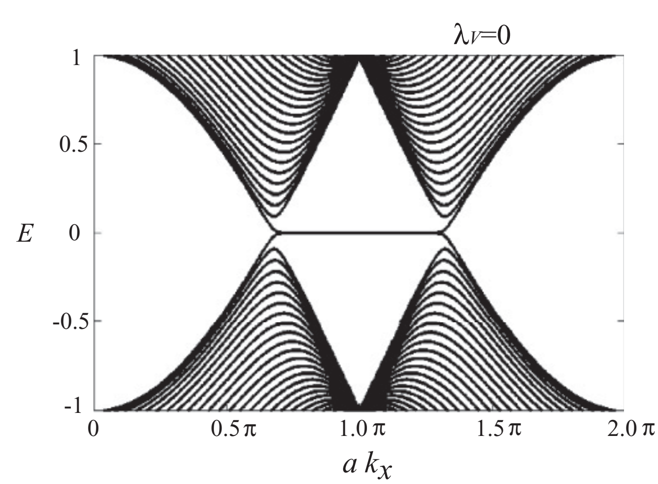

FIG. 3. The energy bands of the SU(1,1) model (16) with zigzag edges along the x direction for $t = 1.0$ and $\lambda_V = 0$ (Hermitian case). Here, a is the lattice constant and k_x the momentum in the x direction. A zero-energy edge state with flat band appears for $2\pi/3 < ak_x < 4\pi/3$.

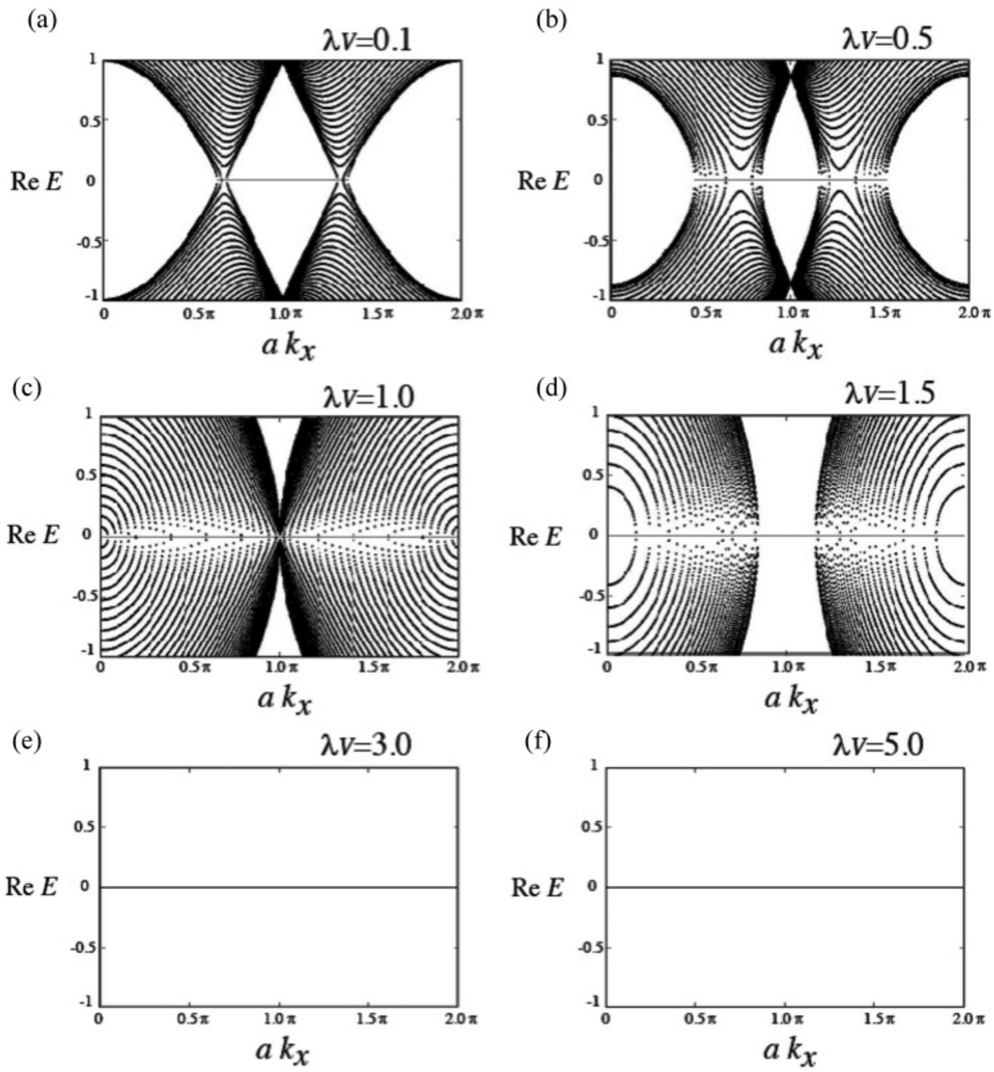

FIG. 4. The real part of the energy bands of the SU(1,1) model (16) with zigzag edges along the x direction. We show the results for $t = 1.0$ and various values of non-Hermitian parameter λ_V. Here, a is the lattice constant and k_x the momentum in the x direction. For weak non-Hermiticity [(a) and (b)], the edge state with $\mathrm{Re}E = 0$ survives around $ak_x \sim \pi$. For large λ_V [(c)–(f)], no edge state with $\mathrm{Re}E = 0$ appears.

(see Figs. 4 and 5). We illustrate the real and the imaginary parts of the energy bands as functions of ak_x in Figs. 4 and 5, respectively. It is clearly seen that the edge state with $\mathrm{Re}E = 0$ persists in the region $2\pi/3 < ak_x < 4\pi/3$ for small λ_V.

B. Winding number and generalized index theorem for non-Hermitian system

From the bulk-edge correspondence, the zero-energy edge state suggests the existence of a topological number responsible for the edge mode. Here, we will see that this is indeed the case and the edge state is characterized by the one-dimensional winding number.

1. Basic property of edge states

In order to make our arguments concrete, we consider the semi-infinite SU(1,1) model on $m > 0$. We perform the inverse Fourier transformation of $H(\boldsymbol{k})$ in Eq. (17) with respect to k_y and denote the resultant Hamiltonian as $H(k_x)_{m,m'}$. The energy spectrum of the system is given by

$$\sum_{m'} H(k_x)_{m,m'}|u(k_x,m')\rangle = E(k_x)|u(k_x,m)\rangle, \tag{20}$$

with

$$|u(k_x,m)\rangle = 0 \tag{21}$$

for $m \leqslant 0$. In the following, we consider k_x as a parameter of the system and treat the model as a one-dimensional system along the y direction. We also restrict our argument on k_x where the bulk energy gap is open in the real part of the energy. The zero-energy edge state satisfies (20) and (21) with $\mathrm{Re}E(k_x) = 0$.

As was shown in Ref. 17, the basic symmetry of the SU(1,1) Hamiltonian is pseudo-anti-Hermiticity given by

$$\sigma_3 H(\boldsymbol{k})^{\dagger}\sigma_3 = -H(\boldsymbol{k}), \tag{22}$$

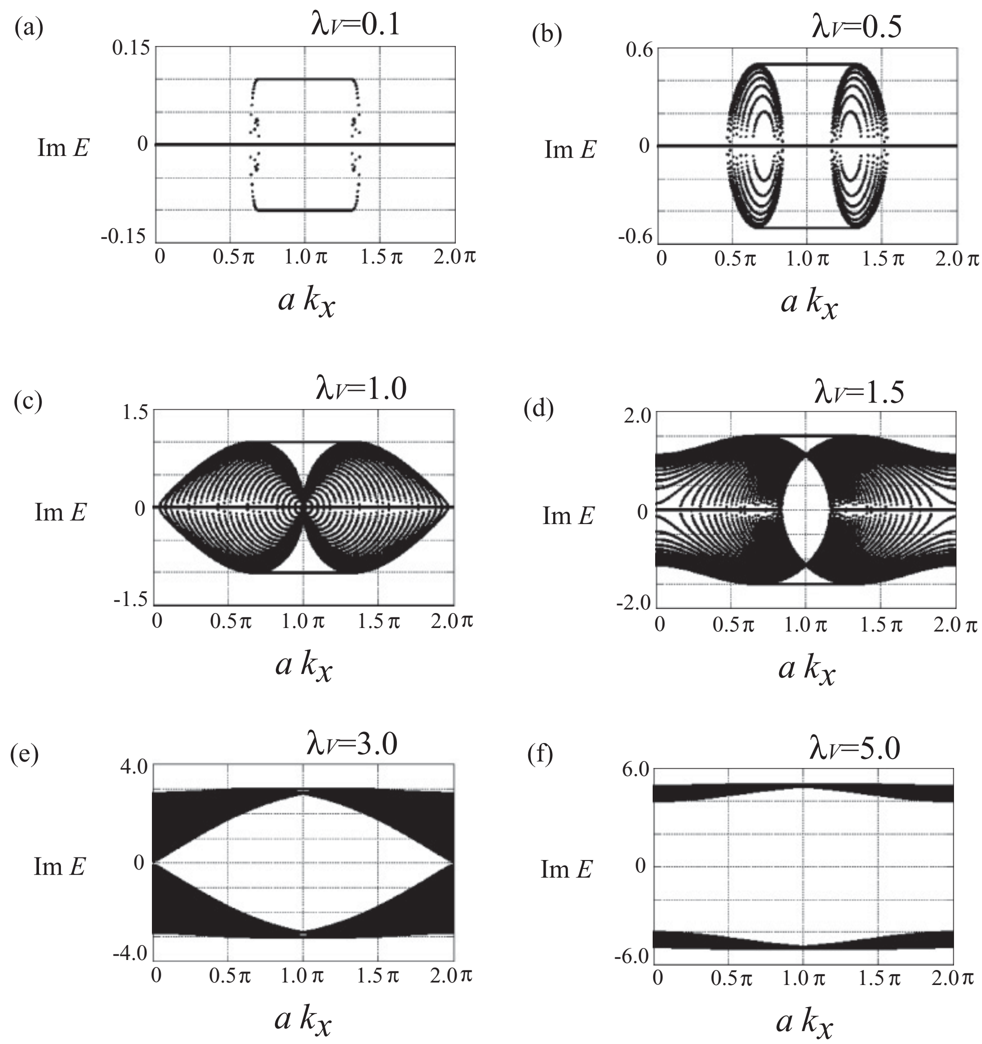

FIG. 5. The imaginary part of the energy bands of the SU(1,1) model (16) with zigzag edges along the x direction. We plot the results for $t = 1.0$ and various values of the non-Hermitian parameter λ_V. Here, a is the lattice constant and k_x the momentum in the x direction. For weak non-Hermiticity [(a) and (b)], there is no imaginary part in the bulk except near the gap-closing points at $ak_x = 2\pi/3$ and $ak_x = 4\pi/3$. The edge states with $\mathrm{Re}E = 0$ [Figs. 4(a) and 4(b)] support the imaginary part in their energy. For large λ_V [(c)–(f)], the bulk states support the imaginary part.

which also implies the pseudo-anti-Hermiticity of the Fourier transformed one

$$\sigma_3[H(k_x)^\dagger]_{m,m'}\sigma_3 = -H(k_x)_{m,m'}. \tag{23}$$

The pseudo-anti-Hermiticity is a key ingredient of our topological argument.

Let us denote the right eigenvectors and the left eigenvectors of $H(k_x)_{m,m'}$ as $|u(k_x,m)\rangle$ and $|u(k_x,m)\rangle\rangle$, respectively:

$$\begin{aligned}\sum_{m'} H(k_x)_{m,m'}|u(k_x,m')\rangle &= E(k_x)|u(k_x,m)\rangle,\\ \sum_{m'}[H(k_x)^\dagger]_{m,m'}|u(k_x,m')\rangle\rangle &= E(k_x)^*|u(k_x,m)\rangle\rangle,\end{aligned} \tag{24}$$

where $|u(k_x,m)\rangle$ and $|u(k_x,m)\rangle\rangle$ are normalized as

$$\sum_m \langle\langle u(k_x,m)|u(k_x,m)\rangle = \sum_m \langle u(k_x,m)|u(k_x,m)\rangle\rangle = 1. \tag{25}$$

From the pseudo-anti-Hermiticity (23), we find that

$$\sum_{m'} H(k_x)_{m,m'}\sigma_3|u(k_x,m')\rangle\rangle = -E(k_x)^*\sigma_3|u(k_x,m)\rangle\rangle. \tag{26}$$

Therefore, the eigenstate $|u(k_x,m)\rangle$ with eigenenergy $E(k_x)$ always comes in pairs with the eigenstate $\sigma_3|u(k_x,m)\rangle\rangle$ with eigenenergy $-E(k_x)^*$. When $\mathrm{Re}E(k_x) \neq 0$, $|u(k_x,m)\rangle$ and $\sigma_3|u(k_x,m)\rangle\rangle$ are independent of each other since they have different energies. On the other hand, for edge states with $\mathrm{Re}E(k_x) = 0$, they are not always independent. Actually, by choosing a proper basis, they can be related to each other as

$$\sigma_3|u(k_x,m)\rangle\rangle = +|u(k_x,m)\rangle \tag{27}$$

or

$$\sigma_3|u(k_x,m)\rangle\rangle = -|u(k_x,m)\rangle, \tag{28}$$

where the overall phase factors of the right-hand sides of (27) and (28) are restricted to ± 1 due to the normalization condition

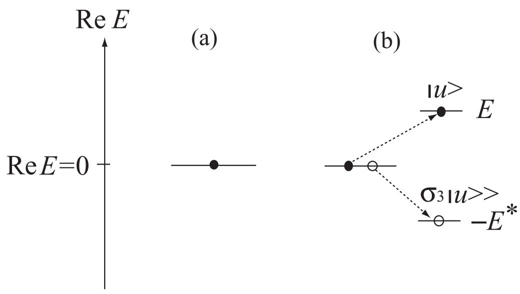

FIG. 6. (a) Topologically protected state with Re$E = 0$. (b) Topologically trivial states with Re$E = 0$. Here, the closed (open) circles at Re$E = 0$ represent states satisfying $\sigma_3|u\rangle\rangle = +|u\rangle$ [Eq. (27)] ($\sigma_3|u\rangle\rangle = -|u\rangle$ [Eq. (28)]). In the latter case [(b)], the state can be nonzero mode since $n_+^0 - n_-^0 = 0$.

(25). We denote the number of the edge states with Re$E(k_x) = 0$ satisfying (27) and (28) as n_+^0 and n_-^0, respectively.

Here, we can show an important property of the edge states: The difference between n_+^0 and n_-^0 does not change its value against perturbation preserving the pseudo-anti-Hermiticity. The reason why $n_+^0 - n_-^0$ is conserved is as follows. For Re$E(k_x) \neq 0$, $|u(k_x,m)\rangle$ and $\sigma_3|u(k_x,m)\rangle\rangle$ are independent, so we can construct another basis from them as

$$|u_\pm(k_x,m)\rangle = \frac{1}{\sqrt{2}}[|u(k_x,m)\rangle\rangle \pm \sigma_3|u(k_x,m)\rangle], \qquad |u_\pm(k_x,m)\rangle\rangle = \frac{1}{\sqrt{2}}[|u(k_x,m)\rangle \pm \sigma_3|u(k_x,m)\rangle\rangle], \tag{29}$$

with

$$\langle\langle u_\pm(k_x,m)|u_\pm(k_x,m)\rangle = 1, \quad \langle\langle u_\pm(k_x,m)|u_\mp(k_x,m)\rangle = 0. \tag{30}$$

Since these states $|u_+(k_x,m)\rangle$ and $|u_-(k_x,m)\rangle$ satisfy Eqs. (27) and (28), respectively,

$$\sigma_3|u_\pm(k_x,m)\rangle\rangle = \pm|u_\pm(k_x,m)\rangle, \tag{31}$$

we have the same number of states with signs $+$ and $-$ in the right-hand side of (31) for Re$E(k_x) \neq 0$. This means that $n_+^0 - n_-^0$ can not change adiabatically: by small perturbation, some of the edge states may acquire a nonzero real part of the energy. If this happens, however, they must be paired with opposite sign in the right-hand side of (31). As a result, the difference between n_+^0 and n_-^0 does not change at all. In Fig. 6, we illustrate two different edge states with Re$E = 0$: one is topologically protected from the above argument and the other topologically trivial.

2. *Winding number*

Now, we introduce a bulk topological number relevant to the present edge mode. To do this, consider the eigenequation for $H(\boldsymbol{k})$ in the momentum space

$$H(\boldsymbol{k})|u_n(\boldsymbol{k})\rangle = E_n(\boldsymbol{k})|u_n(\boldsymbol{k})\rangle, \qquad H(\boldsymbol{k})^\dagger|u_n(\boldsymbol{k})\rangle\rangle = E_n(\boldsymbol{k})^*|u_n(\boldsymbol{k})\rangle\rangle, \tag{32}$$

where n denotes the index labeling different bands. We assume that the system is half-filling and that we have a gap in the real part of energy around Re$E(\boldsymbol{k}) = 0$ for a fixed value of k_x.

From the pseudo-anti-Hermiticity (22), one can say that, if $|u_n(\boldsymbol{k})\rangle$ is a right eigenstate of $H(\boldsymbol{k})$ with Re$E_n(\boldsymbol{k}) > 0$, $\sigma_3|u_n(\boldsymbol{k})\rangle$ is a left eigenstate of $H(\boldsymbol{k})$ with Re$E_n(\boldsymbol{k}) < 0$. In the following, we use a positive (negative) n for the state with Re$E_n(\boldsymbol{k}) > 0$ (Re$E_n(\boldsymbol{k}) < 0$) and set the relation

$$|u_{-n}(\boldsymbol{k})\rangle\rangle = \sigma_3|u_n(\boldsymbol{k})\rangle, \quad E_{-n}(\boldsymbol{k})^* = -E_n(\boldsymbol{k}). \tag{33}$$

The topological number is constructed from the non-Hermitian generalization of the projection operators $\widetilde{\mathcal{P}}_1(\boldsymbol{k})$ and $\widetilde{\mathcal{P}}_2(\boldsymbol{k})$ for occupied bands:[31,32]

$$\widetilde{\mathcal{P}}_1(\boldsymbol{k}) = \sum_{n<0}|u_n(\boldsymbol{k})\rangle\rangle\langle u_n(\boldsymbol{k})|, \qquad \widetilde{\mathcal{P}}_2(\boldsymbol{k}) = \sum_{n<0}|u_n(\boldsymbol{k})\rangle\langle\langle u_n(\boldsymbol{k})|, \qquad [\widetilde{\mathcal{P}}_1(\boldsymbol{k})]^2 = \widetilde{\mathcal{P}}_1(\boldsymbol{k}), \quad [\widetilde{\mathcal{P}}_2(\boldsymbol{k})]^2 = \widetilde{\mathcal{P}}_2(\boldsymbol{k}). \tag{34}$$

From $\widetilde{\mathcal{P}}_1(\boldsymbol{k})$ and $\widetilde{\mathcal{P}}_2(\boldsymbol{k})$, we define the following $\mathcal{Q}$ matrix:

$$\begin{aligned}\widetilde{\mathcal{Q}}(\boldsymbol{k}) &= \mathbf{1} - [\widetilde{\mathcal{P}}_1(\boldsymbol{k}) + \widetilde{\mathcal{P}}_2(\boldsymbol{k})] \\ &= \frac{1}{2}\Bigg(\sum_{n>0}|u_n(\boldsymbol{k})\rangle\rangle\langle u_n(\boldsymbol{k})| - \sum_{n<0}|u_n(\boldsymbol{k})\rangle\rangle\langle u_n(\boldsymbol{k})| \\ &\quad + \sum_{n>0}|u_n(\boldsymbol{k})\rangle\langle\langle u_n(\boldsymbol{k})| - \sum_{n<0}|u_n(\boldsymbol{k})\rangle\langle\langle u_n(\boldsymbol{k})|\Bigg),\end{aligned} \tag{35}$$

where the completeness relation $\sum_n |u_n(\boldsymbol{k})\rangle\rangle\langle u_n(\boldsymbol{k})| = \sum_n |u_n(\boldsymbol{k})\rangle\langle\langle u_n(\boldsymbol{k})| = \mathbf{1}$ was used. One can immediately show that the matrix $\widetilde{\mathcal{Q}}(\boldsymbol{k})$ is Hermitian:

$$\widetilde{\mathcal{Q}}(\boldsymbol{k})^\dagger = \widetilde{\mathcal{Q}}(\boldsymbol{k}). \tag{36}$$

From (33) and (35), we find that $\widetilde{\mathcal{Q}}(\boldsymbol{k})$ and σ_3 anticommute:

$$\{\widetilde{\mathcal{Q}}(\boldsymbol{k}),\sigma_3\} = 0. \tag{37}$$

Since σ_3 is diagonal, Eq. (37) implies that $\widetilde{\mathcal{Q}}(\boldsymbol{k})$ is off diagonal and can be expressed by a complex function $q(\boldsymbol{k})$ as

$$\widetilde{\mathcal{Q}}(\boldsymbol{k}) = \begin{pmatrix} 0 & q(\boldsymbol{k}) \\ q(\boldsymbol{k})^* & 0 \end{pmatrix}. \tag{38}$$

The topological number relevant to our model is the one-dimensional (1D) winding number $w_{1\mathrm{D}}$ defined as

$$w_{1\mathrm{D}}(k_x) = \frac{1}{2\pi i}\int_0^{2\pi} q(\boldsymbol{k})^{-1}\frac{\partial}{\partial k_y}q(\boldsymbol{k})dk_y. \tag{39}$$

By using polar coordinates $q(\boldsymbol{k}) = |q(\boldsymbol{k})|e^{i\alpha(\boldsymbol{k})}$, we obtain

$$\begin{aligned} w_{1\mathrm{D}}(k_x) &= \frac{1}{2\pi}\int_0^{2\pi}\frac{\partial\alpha(\boldsymbol{k})}{\partial k_y}dk_y + \frac{1}{2\pi i}\int_0^{2\pi}\frac{\partial}{\partial k_y}[\ln|q(\boldsymbol{k})|]dk_y \\ &= N \quad (N : \text{integer}),\end{aligned} \tag{40}$$

where we have used the periodicity of $q(\boldsymbol{k})$ with respect to k_y to obtain a quantized value N. The bulk-edge correspondence implies that, if the winding number $w_{1\mathrm{D}}(k_x)$ is nonzero, there is a zero-energy state (in the real part of the energy) on the boundary. We will confirm this numerically in Sec. III C.

3. *Generalized index theorem*

In Sec. III B 2, we argue that the nonzero $w_{1\mathrm{D}}(k_x)$ implies the existence of edge states with Re$E = 0$. At the same time, in Sec. III B 1, we find that the nonzero $n_+^0 - n_-^0$ ensures the robustness of the existence of edge states with $\mathrm{Re}E = 0$. Therefore, it is natural to identify these two quantities $w_{1D}(k_x)$ and $n_+^0 - n_-^0$. Since there is a sign ambiguity for the identification, two possible relations are suggested in the form of the index theorem:

$$n_-^0 - n_+^0 = w_{1D}(k_x) \tag{41}$$

or

$$n_+^0 - n_-^0 = w_{1D}(k_x). \tag{42}$$

Here, note that there are two possible choices of the edge of the system, i.e., the surface of the semi-infinite system on $y > 0$ or that on $y < 0$. The two possible choices of the surface correspond to two possible equalities (41) and (42).

In this paper, we will not prove the generalized index theorems (41) and (42). In Ref. 33, one of the present authors proved a similar generalized index theorem for zero-energy edge states in systems with chiral symmetry. We expect that the generalized index theorem in this case can be proved in a similar manner.

C. Application to SU(1,1) Hamiltonian

Here, we present explicit calculations of the winding number $w_{1D}(k_x)$ for our SU(1,1) Hamiltonian (17). Since we treat k_x as a fixed parameter of the system, it is convenient to write (17) as

$$H(\boldsymbol{k}) = \begin{pmatrix} i\gamma & v + v'e^{ik} \\ v + v'e^{-ik} & -i\gamma \end{pmatrix}, \tag{43}$$

with the identification

$$\gamma = \lambda_V, \quad v = 2t\cos\left(\frac{k_x a}{2}\right), \quad v' = t, \quad k = \frac{\sqrt{3}k_y a}{2}. \tag{44}$$

Let us write (35) as

$$\widetilde{\mathcal{Q}}(\boldsymbol{k}) = \widetilde{\mathcal{Q}}'(\boldsymbol{k}) + \widetilde{\mathcal{Q}}'(\boldsymbol{k})^\dagger, \tag{45}$$

where

$$\widetilde{\mathcal{Q}}'(\boldsymbol{k}) = \frac{1}{2}\left(\sum_{n>0} |u_n(\boldsymbol{k})\rangle\!\rangle\langle u_n(\boldsymbol{k})| - \sum_{n<0} |u_n(\boldsymbol{k})\rangle\!\rangle\langle u_n(\boldsymbol{k})|\right). \tag{46}$$

Then, straightforward diagonalization of (43) gives

$$\begin{aligned}\widetilde{\mathcal{Q}}'(\boldsymbol{k}) &= \frac{1}{2\sqrt{|v+v'e^{ik}|^2-\gamma^2}}\begin{pmatrix} -i\gamma & v + v'e^{ik} \\ v + v'e^{-ik} & i\gamma \end{pmatrix} \\ &= \frac{1}{2\sqrt{|v+v'e^{ik}|^2-\gamma^2}} H(\boldsymbol{k})^\dagger. \end{aligned} \tag{47}$$

From (45) and (47), we obtain

$$\begin{aligned}\widetilde{\mathcal{Q}}(\boldsymbol{k}) &= \frac{1}{2\sqrt{|v+v'e^{ik}|^2-\gamma^2}}[H(\boldsymbol{k})^\dagger + H(\boldsymbol{k})] \\ &= \frac{1}{\sqrt{|v+v'e^{ik}|^2-\gamma^2}}\begin{pmatrix} 0 & v + v'e^{ik} \\ v + v'e^{-ik} & 0 \end{pmatrix}. \end{aligned} \tag{48}$$

Therefore, the winding number $w_{1D}(k_x)$ is evaluated by (39) with $q(\boldsymbol{k}) = \frac{1}{\sqrt{|v+v'e^{ik}|^2-\gamma^2}}(v + v'e^{ik})$. Since only the $(v + v'e^{ik})$ part contributes to the winding number, we have

$$w_{1D}(k_x) = \frac{v'}{2\pi}\int_0^{2\pi} \frac{e^{ik}}{v + v'e^{ik}} dk. \tag{49}$$

Furthermore, changing variable as $z = e^{ik}$ leads to

$$w_{1D}(k_x) = \frac{v'}{2\pi i}\oint \frac{1}{v + v'z} dz, \tag{50}$$

where the integral is taken over a unit circle $|z| = 1$. By using the residue theorem, we reach the final result

$$\begin{aligned} w_{1D}(k_x) &= 1 \quad (|v'| > |v|) \\ &= 0 \quad (|v'| < |v|). \end{aligned} \tag{51}$$

Therefore, the bulk-edge correspondence predicts the existence of the edge state with $\mathrm{Re}E = 0$ if $|v'| > |v|$.

In terms of the original parameters of the Hamiltonian (17), the inequality $|v'| > |v|$ means

$$2\left|\cos\left(\frac{k_x a}{2}\right)\right| < 1. \tag{52}$$

Thus, the edge state with $\mathrm{Re}E = 0$ is predicted in a region of $2\pi/3 < ak_x < 4\pi/3$, provided k_x also satisfies $(2t|\cos(\frac{k_x a}{2})| - t)^2 > \lambda_V^2$ so that the bulk energy gap is open. This prediction is clearly confirmed in Figs. 4 and 5.

IV. SO(3,2) MODEL AND TIME-REVERSAL-INVARIANT CHERN NUMBER

In this section, we examine SO(3,2) Hamiltonians as a higher-symmetric generalization of the SU(1,1) ones examined in Sec. III. As a concrete example, we consider a non-Hermitian generalization of the Luttinger Hamiltonian[6,11] on the square lattice. We find that gapless edge states exist under weak non-Hermiticity. To explain the topological origin of the gapless edge states, we introduce a time-reversal-invariant Chern number inherent to a class of non-Hermitian Hamiltonians based on discrete symmetry of the system. From the bulk-edge correspondence, the time-reversal-invariant Chern number ensures the existence of the gapless edge states in the non-Hermitian system.

A. General Hamiltonian with time-reversal symmetry and pseudo-Hermiticity

We first derive a general 4×4 non-Hermitian Hamiltonian with pseudo-Hermiticity,[34,35] which is invariant under time-reversal symmetry Θ_+ with $\Theta_+^2 = +1$ as well. Such a Hamiltonian belongs to one of the 43 classes of random matrix classification for non-Hermitian systems presented in Ref. 36. Gapless edge states obtained in the following are expected to be robust against disorder in the same class.

A general 4×4 complex Hamiltonian $H(\boldsymbol{k})$ can be represented by a linear combination of the identity matrix, 5 gamma matrices Γ_a, and 10 commutators $\Gamma_{ab} = [\Gamma_a, \Gamma_b]/(2i)$ $(a,b = 1,2,\ldots,5)$:

$$H(\boldsymbol{k}) = h_0(\boldsymbol{k}) + \sum_{a=1}^{5} h_a(\boldsymbol{k})\Gamma_a + \sum_{a<b=1}^{5} h_{ab}(\boldsymbol{k})\Gamma_{ab}, \tag{53}$$

where $h_0(\boldsymbol{k})$, $h_a(\boldsymbol{k})$'s, and $h_{ab}(\boldsymbol{k})$'s are complex functions of $\boldsymbol{k}$. We adopt the following representation of the gamma matrices:

$$\Gamma_1 = \begin{pmatrix} 0 & 1_2 \\ 1_2 & 0 \end{pmatrix}, \quad \Gamma_2 = \begin{pmatrix} 0 & -i1_2 \\ i1_2 & 0 \end{pmatrix},$$
$$\Gamma_\alpha = \begin{pmatrix} \sigma^{\alpha-2} & 0 \\ 0 & -\sigma^{\alpha-2} \end{pmatrix}, \tag{54}$$

where $\alpha = 3,4,5$ and σ^μ ($\mu = 1,2,3$) are the Pauli matrices.[37]

Now, we consider time-reversal symmetry. The time-reversal operator Θ is represented as

$$\Theta = U \cdot K, \tag{55}$$

where U is a unitary operator and K is the complex-conjugate operator. The square of a time-reversal operator is either $+1$ or -1:

$$\Theta_\pm^2 = \pm 1. \tag{56}$$

In the following, we focus on the time-reversal symmetry Θ_+ with $\Theta_+^2 = +1$. For later use, it is convenient to choose U in Θ_+ as $U = \Gamma_1\Gamma_4$. By imposing the time-reversal invariance on $H(\boldsymbol{k})$,

$$\Theta_+ H(-\boldsymbol{k})\Theta_+^{-1} = H(\boldsymbol{k}), \quad \Theta_+ = \Gamma_1\Gamma_4 \cdot K \tag{57}$$

we obtain

$$\begin{aligned} h_0(\boldsymbol{k}) &= h_0(-\boldsymbol{k})^*, \quad h_{(1,2)}(\boldsymbol{k}) = -h_{(1,2)}(-\boldsymbol{k})^*, \\ h_{(3,4,5)}(\boldsymbol{k}) &= h_{(3,4,5)}(-\boldsymbol{k})^*, \\ h_{(12,34,35,45)}(\boldsymbol{k}) &= -h_{(12,34,35,45)}(-\boldsymbol{k})^*, \\ h_{(13,14,15,23,24,25)}(\boldsymbol{k}) &= h_{(13,14,15,23,24,25)}(-\boldsymbol{k})^*. \end{aligned} \tag{58}$$

In addition to the time-reversal invariance, we impose pseudo-Hermiticity on $H(\boldsymbol{k})$,

$$\eta H(\boldsymbol{k})^\dagger \eta^{-1} = H(\boldsymbol{k}), \quad \eta = i\Gamma_2\Gamma_1 \tag{59}$$

with Hermitian matrix η. Here, η is called the metric operator and we have supposed that the metric operator η anticommutes with the time-reversal operation

$$\{\Theta_+,\eta\} = 0, \tag{60}$$

which restricts the allowed form of η. From a proper unitary transformation and rescaling, we can always take the basis in which η is given by $\eta = i\Gamma_2\Gamma_1$. Equation (59) leads to

$$\begin{aligned} h_0(\boldsymbol{k}) &= h_0(\boldsymbol{k})^*, \quad h_{(1,2)}(\boldsymbol{k}) = -h_{(1,2)}(\boldsymbol{k})^*, \\ h_{(3,4,5)}(\boldsymbol{k}) &= h_{(3,4,5)}(\boldsymbol{k})^*, \\ h_{(12,34,35,45)}(\boldsymbol{k}) &= h_{(12,34,35,45)}(\boldsymbol{k})^*, \\ h_{(13,14,15,23,24,25)}(\boldsymbol{k}) &= -h_{(13,14,15,23,24,25)}(\boldsymbol{k})^*. \end{aligned} \tag{61}$$

By combining (58) and (61), $H(\boldsymbol{k})$ is written as

$$\begin{aligned} H(\boldsymbol{k}) = a_0(\boldsymbol{k}) &+ i\sum_{\mu=1,2} b_\mu(\boldsymbol{k})\Gamma_\mu + \sum_{\mu=3,4,5} a_\mu(\boldsymbol{k})\Gamma_\mu \\ &+ \sum_{\mu\nu=12,34,35,45} a_{\mu\nu}(\boldsymbol{k})\Gamma_{\mu\nu} \\ &+ i\sum_{\mu\nu=13,14,15,23,24,25} b_{\mu\nu}(\boldsymbol{k})\Gamma_{\mu\nu}, \end{aligned} \tag{62}$$

where $a_0(\boldsymbol{k})$, $a_\mu(\boldsymbol{k})$'s, $b_\mu(\boldsymbol{k})$'s, $a_{\mu\nu}(\boldsymbol{k})$'s, and $b_{\mu\nu}(\boldsymbol{k})$'s are real functions of $\boldsymbol{k}$, and satisfy

$$\begin{aligned} a_0(\boldsymbol{k}) &= a_0(-\boldsymbol{k}), \quad b_{(1,2)}(\boldsymbol{k}) = b_{(1,2)}(-\boldsymbol{k}), \\ a_{(3,4,5)}(\boldsymbol{k}) &= a_{(3,4,5)}(-\boldsymbol{k}), \\ a_{(12,34,35,45)}(\boldsymbol{k}) &= -a_{(12,34,35,45)}(-\boldsymbol{k}), \\ b_{(13,14,15,23,24,25)}(\boldsymbol{k}) &= -b_{(13,14,15,23,24,25)}(-\boldsymbol{k}). \end{aligned} \tag{63}$$

B. SO(3,2) Luttinger model and edge state

In order to have real eigenenergies in non-Hermitian systems, PT symmetry plays crucial roles as pointed out by Bender *et al.*[38–40] Following the arguments by Bender *et al.*, we impose the inversion symmetry on $H(\boldsymbol{k})$ in Eq. (62):

$$H(-\boldsymbol{k}) = H(\boldsymbol{k}). \tag{64}$$

From Eqs. (62)–(64), we obtain the following SO(3,2) Hamiltonian:[17]

$$H(\boldsymbol{k}) = a_0(\boldsymbol{k}) + i\sum_{\mu=1,2} b_\mu(\boldsymbol{k})\Gamma_\mu + \sum_{\mu=3,4,5} a_\mu(\boldsymbol{k})\Gamma_\mu, \tag{65}$$

with real even functions $a_0(\boldsymbol{k})$, $a_\mu(\boldsymbol{k})$'s, and $b_\mu(\boldsymbol{k})$'s. The eigenenergies are

$$\begin{aligned} E_\pm(\boldsymbol{k}) \\ = a_0(\boldsymbol{k}) \pm \sqrt{a_3(\boldsymbol{k})^2 + a_4(\boldsymbol{k})^2 + a_5(\boldsymbol{k})^2 - b_1(\boldsymbol{k})^2 - b_2(\boldsymbol{k})^2}, \end{aligned} \tag{66}$$

each of which is doubly degenerate. As is expected from PT symmetry, these eigenenergies are real if $a_3(\boldsymbol{k})^2 + a_4(\boldsymbol{k})^2 + a_5(\boldsymbol{k})^2 > b_1(\boldsymbol{k})^2 + b_2(\boldsymbol{k})^2$.

To realize such an SO(3,2) model, we generalize the SO(5) Luttinger Hamiltonian[6,11] on the square lattice into a non-Hermitian form

$$H(\boldsymbol{k}) = \epsilon(\boldsymbol{k}) + V\sum_{a=3,4,5} d_a(\boldsymbol{k})\Gamma_a + iV\sum_{a=1,2} d_a\Gamma_a, \tag{67}$$

where

$$\begin{aligned} \epsilon(\boldsymbol{k}) &= t(-2\cos k_x - 2\cos k_y + e_s), \\ d_3(\boldsymbol{k}) &= -\sqrt{3}\sin k_x \sin k_y, \\ d_4(\boldsymbol{k}) &= \sqrt{3}(\cos k_x - \cos k_y), \\ d_5(\boldsymbol{k}) &= 2 - e_s - \cos k_x - \cos k_y, \end{aligned} \tag{68}$$

with $\boldsymbol{k} = (k_x,k_y)$. The imaginary unit i in the last term in the right-hand side of (67) is absent in the original SO(5) Luttinger Hamiltonian. For simplicity, we take d_1 and d_2 to

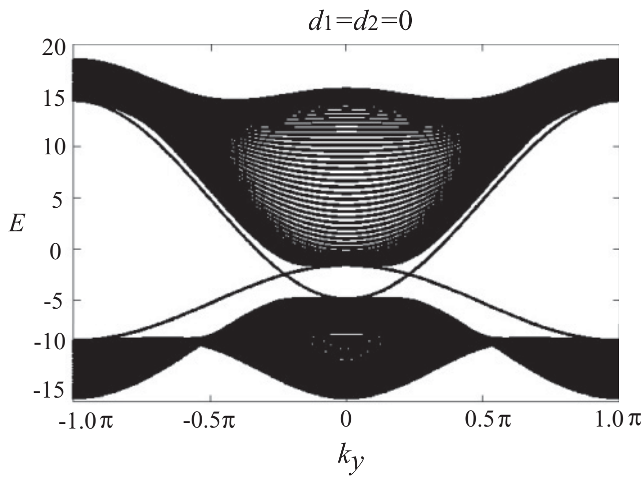

FIG. 7. The energy bands of the SO(3,2) Luttinger Hamiltonian (67) with open boundary condition in the x direction for $t = 1.0$, $V = 4.0$, $e_s = 0.5$, and $d_1 = d_2 = 0$ (Hermitian case). Here, k_y is the momentum in the y direction. Two gapless helical edge states appear on each edge.

be real constants. Here, $e_s \equiv \langle k_z^2 \rangle$, where $\langle \cdots \rangle$ represents the expectation value in the lowest band.[41] The eigenenergies are

$$E_\pm(\boldsymbol{k}) = \epsilon(\boldsymbol{k}) \pm V\sqrt{d_3(\boldsymbol{k})^2 + d_4(\boldsymbol{k})^2 + d_5(\boldsymbol{k})^2 - d_1^2 - d_2^2}, \tag{69}$$

each of which is doubly degenerate.

Now, we examine edge states of this model. We put the system on a cylinder with the periodic boundary condition in the y direction and open boundary condition in the x direction, and study the quasiparticle spectrum numerically.

First, we illustrate the quasiparticle spectrum for the Hermitian case with $d_1 = d_2 = 0$. The energy bands in this case are shown in Fig. 7. In the gap of the bulk bands, there exist doubly degenerate edge bands. The existence of the gapless edge bands is explained by the so-called spin Chern number.[11] When $d_1 = d_2 = 0$, in addition to the $\Theta_+^2 = +1$ time-reversal symmetry (57), the Hamiltonian (67) has the following $\Theta_-^2 = -1$ time-reversal symmetry:

$$\Theta_- H(-\boldsymbol{k})\Theta_-^{-1} = H(\boldsymbol{k}), \quad \Theta_- = \Gamma_2\Gamma_4 \cdot K. \tag{70}$$

Moreover, since $H(\boldsymbol{k}) = H^\dagger(\boldsymbol{k})$ for $d_1 = d_2 = 0$, the pseudo-Hermiticity (59) reduces to

$$[H(\boldsymbol{k}),\eta] = 0. \tag{71}$$

Thus, in this special case, η becomes a conserved quantity. Indeed, the operator η is identified with the pseudo-spin operator S_z in the Luttinger model,[11] the eigenvalue of which is either $+1$ or -1. In Ref. 11, the spin Chern number C_s was defined by using the pseudo-spin S_z and the time-reversal symmetry Θ_-, and it was shown that $C_s = 2$ if $0 < e_s < 4$. Therefore, the existence of the gapless edge bands is ensured by the spin Chern number.

Let us now examine the non-Hermitian case. We show the real and the imaginary parts of the energy bands as functions of k_y for various (d_1,d_2)'s in Figs. 8 and 9, respectively. Interestingly, the gapless edge bands persist in the real part even in the presence of the non-Hermiticity (d_1,d_2) [Figs. 8(a) and 8(b)], although they have a small imaginary part at the same time [Figs. 9(a) and 9(b)]. Since the non-Hermiticity breaks both of the time-reversal invariance for Θ_- and the rotational invariance for S_z, such gapless modes can not be explained by the spin Chern number. The topological origin of the gapless edge mode will be discussed in the next section. If we further increase (d_1,d_2), the bulk gap closes, and only remnants of the edge states are observed [Figs. 8(c)–8(f)].

C. Time-reversal-invariant Chern number

In Sec. IV B, we showed that there exist gapless edge states in the SO(3,2) non-Hermitian model. Here, we will discuss the topological origin of these gapless edge states.

1. Generalized Kramers theorem

First of all, we examine general properties of eigenstates for the non-Hermitian Hamiltonian. Let us denote the right eigenvectors and the left eigenvectors of a non-Hermitian Hamiltonian $H(\boldsymbol{k})$ as $|u_n(\boldsymbol{k})\rangle$ and $|u_n(\boldsymbol{k})\rangle\rangle$, respectively:

$$\begin{aligned} H(\boldsymbol{k})|u_n(\boldsymbol{k})\rangle &= E_n(\boldsymbol{k})|u_n(\boldsymbol{k})\rangle, \\ H(\boldsymbol{k})^\dagger|u_n(\boldsymbol{k})\rangle\rangle &= E_n(\boldsymbol{k})^*|u_n(\boldsymbol{k})\rangle\rangle, \end{aligned} \tag{72}$$

where $|u_n(\boldsymbol{k})\rangle$ and $|u_n(\boldsymbol{k})\rangle\rangle$ are normalized as

$$\langle\langle u_m(\boldsymbol{k})|u_n(\boldsymbol{k})\rangle = \langle u_m(\boldsymbol{k})|u_n(\boldsymbol{k})\rangle\rangle = \delta_{mn}. \tag{73}$$

The eigenstates $|u_n(\boldsymbol{k})\rangle$ and $|u_n(\boldsymbol{k})\rangle\rangle$ satisfying (73) are called the biorthonormal basis.

Now, suppose that $H(\boldsymbol{k})$ is pseudo-Hermitian:

$$H(\boldsymbol{k})^\dagger = \eta H(\boldsymbol{k})\eta^{-1}. \tag{74}$$

From the pseudo-Hermiticity, the first equation of (72) is rewritten as

$$H(\boldsymbol{k})^\dagger \eta|u_n(\boldsymbol{k})\rangle = E_n(\boldsymbol{k})\eta|u_n(\boldsymbol{k})\rangle. \tag{75}$$

Therefore, $\eta|u_n(\boldsymbol{k})\rangle$ is an eigenstate of $H(\boldsymbol{k})^\dagger$ and it can be expanded as

$$\eta|u_n(\boldsymbol{k})\rangle = \sum_m |u_m(\boldsymbol{k})\rangle\rangle c_{mn}(\boldsymbol{k}). \tag{76}$$

By applying $\langle u_m(\boldsymbol{k})|$ from the left, we obtain

$$c_{mn}(\boldsymbol{k}) = \langle u_m(\boldsymbol{k})|\eta|u_n(\boldsymbol{k})\rangle. \tag{77}$$

Since η is Hermitian, $c_{mn}(\boldsymbol{k})$ is also Hermitian with respect to the indices m and n. Thus, it can be diagonalized by a unitary matrix G:

$$\sum_{lk} G_{ml}(\boldsymbol{k})^\dagger c_{lk}(\boldsymbol{k}) G_{kn}(\boldsymbol{k}) = \lambda_m(\boldsymbol{k})\delta_{mn} \tag{78}$$

with real $\lambda_n(\boldsymbol{k})$. The eigenvalue $\lambda_n(\boldsymbol{k})$ is not zero since $c_{mn}(\boldsymbol{k})$ is invertible. Taking the following new biorthonormal

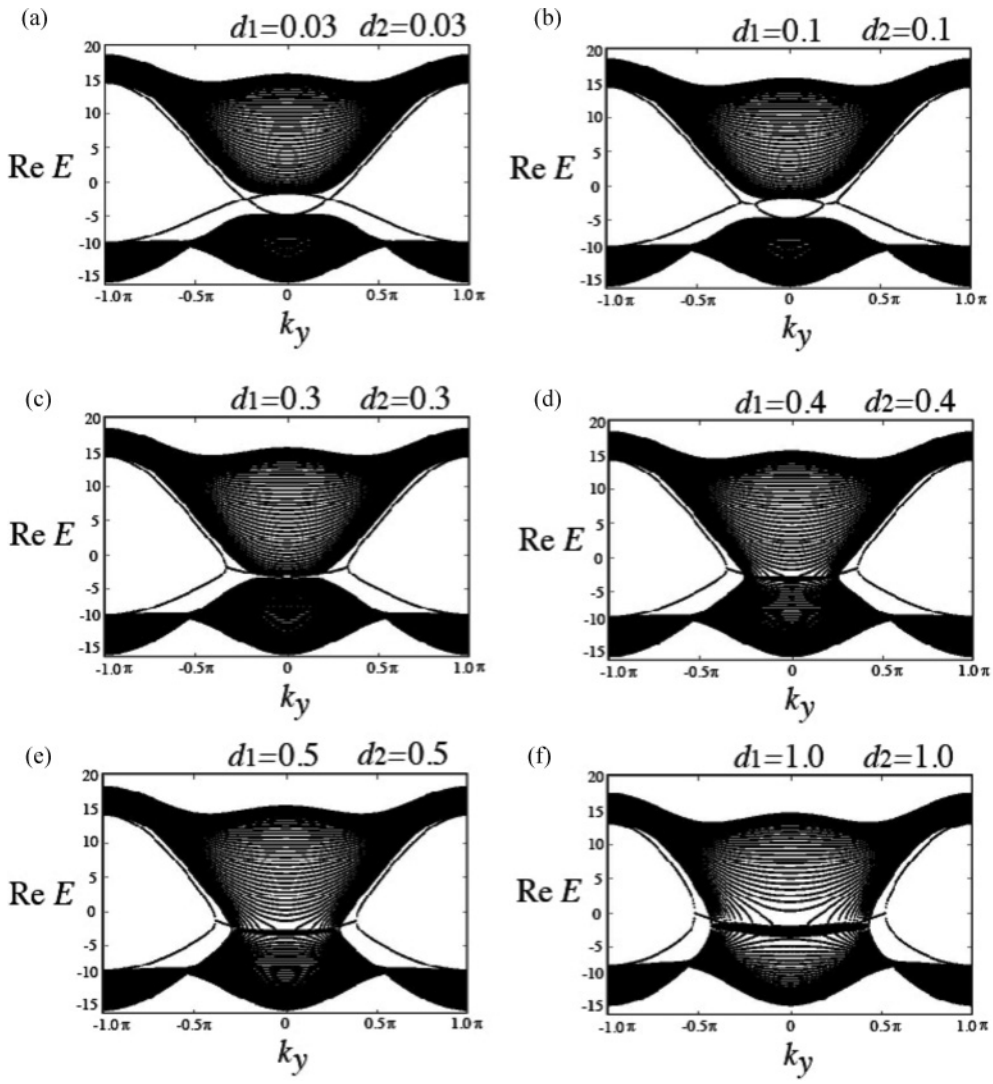

FIG. 8. The real part of the energy bands of the SO(3,2) Luttinger Hamiltonian (67) with the open boundary condition in the x direction. We plot the results for $t = 1.0$, $V = 4.0$, $e_s = 0.5$, and various values of the non-Hermitian parameters (d_1,d_2). Here, k_y is the momentum in the y direction. For weak non-Hermiticity [(a) and (b)], two gapless helical edge modes survive. When the bulk gap in the real part of the energy closes [(c) and (d)], the topological number $C_{\rm TRI}$ is not well defined. In this parameter region, only remnants of the edge states are observed.

basis

$$|\phi_n(\boldsymbol{k})\rangle = \sum_m |u_m(\boldsymbol{k})\rangle G_{mn}(\boldsymbol{k})/\sqrt{|\lambda_n(\boldsymbol{k})|},$$
$$|\phi_n(\boldsymbol{k})\rangle\!\rangle = \sum_m |u_m(\boldsymbol{k})\rangle\!\rangle G_{mn}(\boldsymbol{k})\sqrt{|\lambda_n(\boldsymbol{k})|}, \tag{79}$$

with $\langle\phi_m(\boldsymbol{k})|\phi_n(\boldsymbol{k})\rangle\!\rangle = \langle\!\langle\phi_m(\boldsymbol{k})|\phi_n(\boldsymbol{k})\rangle = \delta_{mn}$, we have

$$\eta|\phi_n(\boldsymbol{k})\rangle = \mathrm{sgn}[\lambda_n(\boldsymbol{k})]|\phi_n(\boldsymbol{k})\rangle\!\rangle. \tag{80}$$

Because of the continuity of the wave function, $\mathrm{sgn}[\lambda_n(\boldsymbol{k})]$ does not change in the whole region of the momentum space. Thus, the states in the new basis are classified into two, i.e., states with

$$\eta|\phi_n(\boldsymbol{k})\rangle = |\phi_n(\boldsymbol{k})\rangle\!\rangle \tag{81}$$

and those with

$$\eta|\phi_n(\boldsymbol{k})\rangle = -|\phi_n(\boldsymbol{k})\rangle\!\rangle. \tag{82}$$

Here, we should note that the new bases $|\phi_n(\boldsymbol{k})\rangle$ are no longer eigenstates of $H(\boldsymbol{k})$ unless $E_n(\boldsymbol{k})$ is real. Indeed, the right-hand side of (79) mixes the eigenstates with $E_n(\boldsymbol{k})$ and those with $E_n(\boldsymbol{k})^*$. However, the mixed states have a common real part of the energy. Therefore, even if the bulk energy $E_n(\boldsymbol{k})$ is not real, the structure of the real part of the eigenenergy remains the same in this basis.

If $H(\boldsymbol{k})$ is invariant under the time-reversal symmetry Θ_+ with $\Theta_+^2 = +1$ and $\{\Theta_+,\eta\} = 0$, we have an additional structure, i.e., the generalized Kramers degeneracy.[17] Let $|\phi_n^{(+)}(\boldsymbol{k})\rangle$ be a wave function satisfying Eq. (81):

$$\eta|\phi_n^{(+)}(\boldsymbol{k})\rangle = |\phi_n^{(+)}(\boldsymbol{k})\rangle\!\rangle, \tag{83}$$

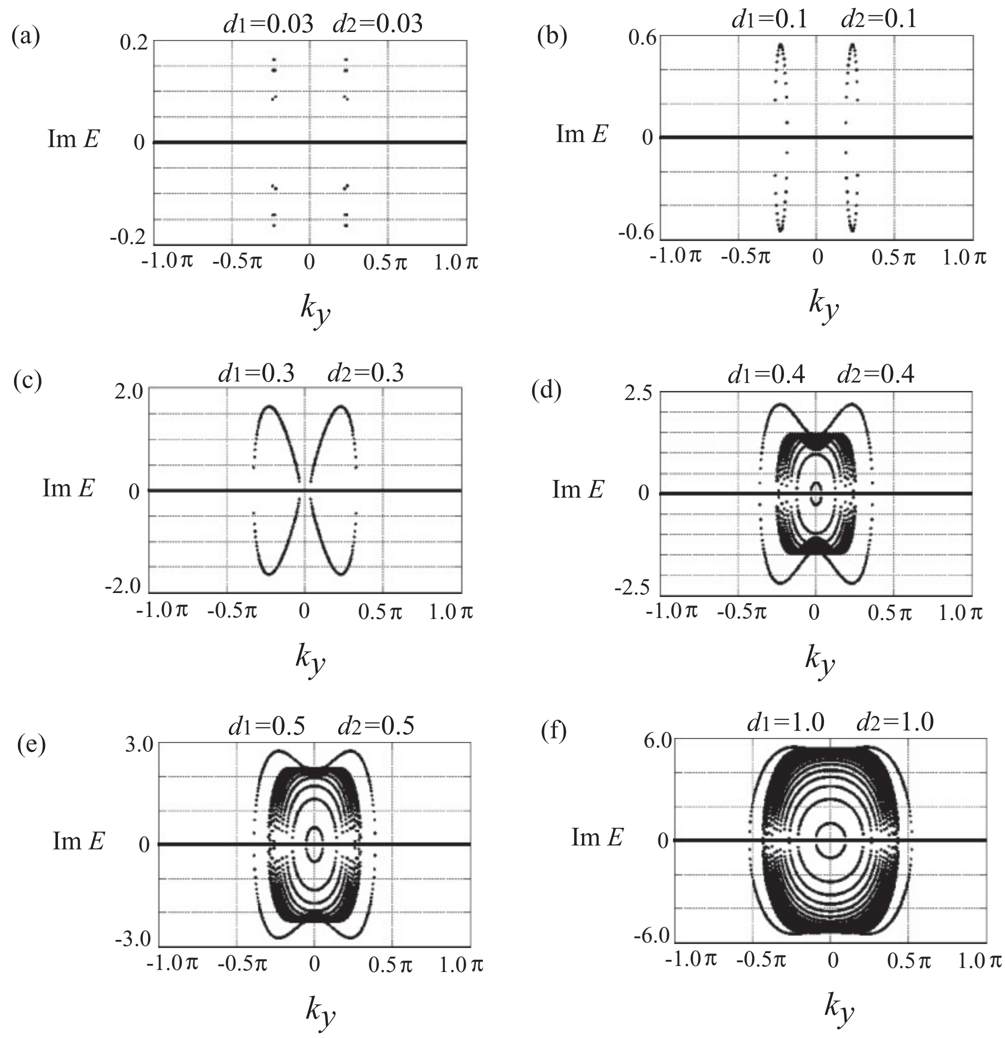

FIG. 9. The imaginary part of the energy bands of the SO(3,2) Luttinger Hamiltonian (67) with the open boundary condition in the x direction. We plot the results for $t=1.0$, $V=4.0$, $e_s=0.5$, and various values of the non-Hermitian parameters (d_1,d_2). Here, k_y is the momentum in the y direction. For weak non-Hermiticity [(a) and (b)], there is no imaginary part in the bulk bands. Only the edge states with $\mathrm{Re}E=0$ [Figs. 8(a) and 8(b)] support the imaginary part in their energy. When the bulk gap in the real part of the energy closes [Figs. 8(c) and 8(d)], the bulk states also support the imaginary part as well.

with

$$\langle\phi_m^{(+)}(\boldsymbol{k})|\phi_n^{(+)}(\boldsymbol{k})\rangle\!\rangle = \langle\!\langle\phi_m^{(+)}(\boldsymbol{k})|\phi_n^{(+)}(\boldsymbol{k})\rangle = \delta_{mn}. \tag{84}$$

The generalized Kramers partner $|\phi_n^{(-)}(\boldsymbol{k})\rangle$ is given by

$$|\phi_n^{(-)}(\boldsymbol{k})\rangle = e^{i\theta_n(\boldsymbol{k})}\Theta\eta^{-1}|\phi_n^{(+)}(-\boldsymbol{k})\rangle\!\rangle, \tag{85}$$

with a phase factor $\theta_n(\boldsymbol{k})$, and the corresponding left state is

$$|\phi_n^{(-)}(\boldsymbol{k})\rangle\!\rangle = e^{i\theta_n(\boldsymbol{k})}\Theta\eta^{-1}|\phi_n^{(+)}(-\boldsymbol{k})\rangle, \tag{86}$$

with

$$\langle\phi_m^{(-)}(\boldsymbol{k})|\phi_n^{(-)}(\boldsymbol{k})\rangle\!\rangle = \langle\!\langle\phi_m^{(-)}(\boldsymbol{k})|\phi_n^{(-)}(\boldsymbol{k})\rangle = \delta_{mn}. \tag{87}$$

The generalized Kramers pairs $|\phi_n^{(\pm)}(\boldsymbol{k})\rangle$ are independent of each other.[17] Actually, it is found easily that at time-reversal-invariant momenta $\boldsymbol{k}=\bar{\Gamma}_i$ satisfying $-\bar{\Gamma}_i=\bar{\Gamma}_i+\boldsymbol{G}$ with a reciprocal vector $\boldsymbol{G}$, these generalized Kramers pairs are orthogonal to each other:

$$\langle\!\langle\phi_n^{(+)}(\bar{\Gamma}_i)|\phi_n^{(-)}(\bar{\Gamma}_i)\rangle = 0 \tag{88}$$

since we have

$$\begin{aligned}
\langle\!\langle\phi_n^{(+)}(\bar{\Gamma}_i)|\phi_n^{(-)}(\bar{\Gamma}_i)\rangle &= e^{i\theta_n(\bar{\Gamma}_i)}\langle\!\langle\phi_n^{(+)}(\bar{\Gamma}_i)|\Theta\eta^{-1}|\phi_n^{(+)}(\bar{\Gamma}_i)\rangle\!\rangle\\
&= e^{i\theta_n(\bar{\Gamma}_i)}\langle\!\langle\Theta^2\eta^{-1}\phi_n^{(+)}(\bar{\Gamma}_i)|\Theta\phi_n^{(+)}(\bar{\Gamma}_i)\rangle\!\rangle\\
&= e^{i\theta_n(\bar{\Gamma}_i)}\langle\!\langle\phi_n^{(+)}(\bar{\Gamma}_i)|\eta^{-1}\Theta\phi_n^{(+)}(\bar{\Gamma}_i)\rangle\!\rangle\\
&= -e^{i\theta_n(\bar{\Gamma}_i)}\langle\!\langle\phi_n^{(+)}(\bar{\Gamma}_i)|\Theta\eta^{-1}\phi_n^{(+)}(\bar{\Gamma}_i)\rangle\!\rangle\\
&= -\langle\!\langle\phi_n^{(+)}(\bar{\Gamma}_i)|\phi_n^{(-)}(\bar{\Gamma}_i)\rangle.
\end{aligned} \tag{89}$$

We also find that the generalized Kramers partner $|\phi_n^{(-)}(\boldsymbol{k})\rangle$ satisfies (82):

$$\begin{aligned}
\eta|\phi_n^{(-)}(\boldsymbol{k})\rangle &= -e^{i\theta_n(\boldsymbol{k})}\Theta|\phi_n^{(+)}(-\boldsymbol{k})\rangle\!\rangle\\
&= -e^{i\theta_n(\boldsymbol{k})}\Theta\eta^{-1}|\phi_n^{(+)}(-\boldsymbol{k})\rangle = -|\phi_n^{(-)}(\boldsymbol{k})\rangle\!\rangle.
\end{aligned} \tag{90}$$

Namely, in the presence of the time-reversal symmetry with $\Theta_+^2 = +1$ and $\{\eta,\Theta_+\} = 0$, the states with (81) are paired with those with (82). As is shown below, this structure enables us to introduce a nontrivial Chern number even for the time-reversal-invariant system.

2. Chern numbers for non-Hermitian systems

Here, we generalize the Chern number for non-Hermitian systems. For non-Hermitian systems, the gauge potential $A_i(\boldsymbol{k})$ is introduced as follows:[18,42]

$$A_i(\boldsymbol{k}) = i \sum_{\mathrm{Re}E_n(\boldsymbol{k})<E} \langle\langle u_n(\boldsymbol{k})|\frac{\partial}{\partial k_i}|u_n(\boldsymbol{k})\rangle, \tag{91}$$

where $|u_n(\boldsymbol{k})\rangle$ denotes the right eigenstate of $H(\boldsymbol{k})$ and $|u_n(\boldsymbol{k})\rangle\rangle$ the corresponding left eigenstate. Here, we suppose that there is a band gap at E in the real part, so no momentum $\boldsymbol{k}$ satisfies $\mathrm{Re}E_n(\boldsymbol{k}) = E$. The gauge potential $A_i(\boldsymbol{k})$ is well defined in the whole region of the momentum space under this assumption. The Chern number C is defined as

$$C = \frac{1}{2\pi}\int\int_{\mathrm{FBZ}} dk_x\, dk_y\, F_{xy}(\boldsymbol{k}), \tag{92}$$

where $F_{xy}(\boldsymbol{k})$ is the field strength of the gauge potential $A_i(\boldsymbol{k})$,

$$F_{xy}(\boldsymbol{k}) = \frac{\partial A_y(\boldsymbol{k})}{\partial k_x} - \frac{\partial A_x(\boldsymbol{k})}{\partial k_y}, \tag{93}$$

and the integration is performed in the first Brillouin zone (FBZ). In a manner similar to Hermitian systems, one can show that C is quantized and takes only integer values: the Chern number (92) counts vorticities of wave functions in the first Brillouin zone.[14] By the gauge transformations $|u_n'(\boldsymbol{k})\rangle = e^{i\alpha(\boldsymbol{k})}|u_n(\boldsymbol{k})\rangle$ and $|u_n'(\boldsymbol{k})\rangle\rangle = e^{i\alpha(\boldsymbol{k})}|u_n(\boldsymbol{k})\rangle\rangle$, the gauge potential $A_i(\boldsymbol{k})$ is transformed as

$$A_i(\boldsymbol{k})' = A_i(\boldsymbol{k}) - \frac{\partial\alpha(\boldsymbol{k})}{\partial k_i}, \tag{94}$$

where the normalization condition (73) was used. As was shown in Ref. 14, the Chern number C reduces to the line integral of the second term of (94) around the zeros of the wave function

$$\frac{1}{2\pi}\oint \frac{\partial\alpha(\boldsymbol{k})}{\partial \boldsymbol{k}}\cdot d\boldsymbol{k}, \tag{95}$$

which counts the vorticity of the wave function in the first Brillouin zone.[14]

When the system is time-reversal invariant, one can show that the Chern number C is always zero. Thus, we can not use the Chern number itself to characterize topological phases for time-reversal-invariant systems. However, if the system is pseudo-Hermitian as well and the time-reversal symmetry Θ_+ satisfies $\Theta_+^2 = +1$ and $\{\eta,\Theta_+\} = 0$, one can define a different Chern number, which can be nontrivial even in the presence of the time-reversal invariance. The key structure is the generalized Kramers pairs explained in the preceding section. Under the above assumption for Θ_+ and η, one can take the following basis:

$$\eta|\phi_n^{(\pm)}(\boldsymbol{k})\rangle = \pm|\phi_n^{(\pm)}(\boldsymbol{k})\rangle\rangle, \tag{96}$$

with

$$\langle\phi_m^{(\pm)}(\boldsymbol{k})|\phi_n^{(\pm)}(\boldsymbol{k})\rangle\rangle = \langle\langle\phi_m^{(\pm)}(\boldsymbol{k})|\phi_n^{(\pm)}(\boldsymbol{k})\rangle = \delta_{mn}. \tag{97}$$

Here, the states $|\phi_n^{(\pm)}(\boldsymbol{k})\rangle$ form the generalized Kramers pair

$$\begin{aligned} |\phi_n^{(-)}(\boldsymbol{k})\rangle &= e^{i\theta_n(\boldsymbol{k})}\Theta\eta^{-1}|\phi_n^{(+)}(-\boldsymbol{k})\rangle\rangle, \\ |\phi_n^{(-)}(\boldsymbol{k})\rangle\rangle &= e^{i\theta_n(\boldsymbol{k})}\Theta\eta^{-1}|\phi_n^{(+)}(-\boldsymbol{k})\rangle. \end{aligned} \tag{98}$$

Using the sign difference of the right-hand side of (96), we can introduce the following two different gauge potentials:

$$A_i^{(\pm)}(\boldsymbol{k}) = i\sum_{\mathrm{Re}E_n(\boldsymbol{k})<E} \langle\langle\phi_n^{(\pm)}(\boldsymbol{k})|\frac{\partial}{\partial k_i}|\phi_n^{(\pm)}(\boldsymbol{k})\rangle, \tag{99}$$

and the corresponding Chern numbers

$$C^{(\pm)} = \frac{1}{2\pi}\int\int_{\mathrm{FBZ}} dk_x\, dk_y\, F_{xy}^{(\pm)}(\boldsymbol{k}), \tag{100}$$

with

$$F_{xy}^{(\pm)}(\boldsymbol{k}) = \frac{\partial A_y^{(\pm)}(\boldsymbol{k})}{\partial k_x} - \frac{\partial A_x^{(\pm)}(\boldsymbol{k})}{\partial k_y}. \tag{101}$$

As we mentioned in the preceding section, if $E_n(\boldsymbol{k})$ is not real, the states $|\phi_n^{(\pm)}(\boldsymbol{k})\rangle$ are not eigenstates of $H(\boldsymbol{k})$ in general. However, for the real part of the eigenenergy, $|\phi_n^{(\pm)}(\boldsymbol{k})\rangle$ has the same structure as the eigenstate of $H(\boldsymbol{k})$. Thus, the summation in Eq. (99) is well defined. It is also found that

$$C = C^{(+)} + C^{(-)}. \tag{102}$$

Under the time-reversal transformation, these Chern numbers transform as $C^{(\pm)} \to -C^{(\mp)}$. Thus, the time-reversal invariance implies that $C = C^{(+)} + C^{(-)} = 0$. On the other hand, the time-reversal-invariant combination

$$C_{\mathrm{TRI}} = \frac{C^{(+)} - C^{(-)}}{2} \tag{103}$$

can be nonzero. We call C_{TRI} the time-reversal-invariant Chern number. In Secs. IV C 3 and V, we will see that the time-reversal-invariant Chern number characterizes the gapless edge state for a class of non-Hermitian systems.

3. Application to SO(3,2) model

Let us now examine C_{TRI} for the SO(3,2) model (65). Below, we suppose that we have a gap around $E_-(\boldsymbol{k})$ and $E_+(\boldsymbol{k})$, and that the system is half-filling. In this model, two right eigenstates $|u_-^{(+)}(\boldsymbol{k})\rangle$ and $|u_-^{(-)}(\boldsymbol{k})\rangle$ with the negative eigenenergy $E_-(\boldsymbol{k})$ are

$$\begin{aligned} |u_-^{(+)}(\boldsymbol{k})\rangle &= \frac{1}{\sqrt{2E(E-a_5)}}\begin{pmatrix} a_5 - E \\ a_3 + ia_4 \\ ib_1 - b_2 \\ 0 \end{pmatrix}, \\ |u_-^{(-)}(\boldsymbol{k})\rangle &= \frac{1}{\sqrt{2E(E-a_5)}}\begin{pmatrix} 0 \\ ib_1 + b_2 \\ -a_3 + ia_4 \\ a_5 - E \end{pmatrix}, \end{aligned} \tag{104}$$

where $E \equiv \sqrt{a_3^2 + a_4^2 + a_5^2 - b_1^2 - b_2^2}$. They form the generalized Kramers pair.

Here, we present explicit calculations of the time-reversal-invariant Chern number for SO(3,2) Hamiltonians (65). By substituting (104) into (99), we obtain

$$\begin{aligned}A_i^{(+)}(\boldsymbol{k}) &= \frac{i}{2E(E-a_5)}\left[(E-a_5)\frac{\partial}{\partial k_i}(E-a_5)+(a_3-ia_4)\frac{\partial}{\partial k_i}(a_3+ia_4)+(ib_1+b_2)\frac{\partial}{\partial k_i}(ib_1-b_2)\right]\\ &\quad + i\frac{\partial}{\partial k_i}\left[\ln\left(\frac{1}{\sqrt{2E(E-a_5)}}\right)\right],\\ A_i^{(-)}(\boldsymbol{k}) &= \frac{i}{2E(E-a_5)}\left[(E-a_5)\frac{\partial}{\partial k_i}(E-a_5)+(a_3+ia_4)\frac{\partial}{\partial k_i}(a_3-ia_4)+(ib_1-b_2)\frac{\partial}{\partial k_i}(ib_1+b_2)\right]\\ &\quad + i\frac{\partial}{\partial k_i}\left[\ln\left(\frac{1}{\sqrt{2E(E-a_5)}}\right)\right].\end{aligned} \tag{105}$$

From (105), we find

$$A_i^{(-)}(\boldsymbol{k}) = [A_i^{(+)}(-\boldsymbol{k})]^*, \tag{106}$$

from which we can show $C = C^{(+)} + C^{(-)} = 0$ explicitly.

To evaluate the time-reversal-invariant Chern number, we adiabatically deform the Hamiltonian of the system without gap closing in the real part of the bulk energy. This process does not change the time-reversal-invariant Chern number. In particular, to calculate the time-reversal-invariant Chern number for weak non-Hermiticity in Figs. 8(a) and 8(b), we decrease the non-Hermiticity (d_1,d_2) adiabatically as $d_i \to 0$ $(i = 1,2)$. In this particular limit, we find that the time-reversal-invariant Chern number C_{TRI} coincides with the spin Chern number C_s in Ref. 11. Therefore, from the adiabatic continuity, we obtain

$$C_{\mathrm{TRI}} = 2 \tag{107}$$

for the model in Fig. 8. This means that the existence of the gapless edge states in Fig. 8 is ensured by the nonzero value of C_{TRI}. Here, we should emphasize that the spin Chern number itself is not well defined once the non-Hermiticity (d_1,d_2) is turned on. On the other hand, the time-reversal-invariant Chern number C_{TRI} is well defined even in the presence of the non-Hermiticity.

V. NON-HERMITIAN KANE-MELE MODEL

So far, we argued systems with imaginary onsite potentials. In this section, we consider a system in which the non-Hermiticity is caused by asymmetric hopping integrals. Consider the following non-Hermitian version of the Kane-Mele model:[7,15]

$$H = H_K + H_V + H_{\mathrm{SO}} + \widetilde{H}_R, \tag{108}$$

where

$$\begin{aligned} H_K &= t\sum_{\langle i,j\rangle}(c_i^\dagger c_j + \mathrm{H.c.}), \quad H_V = \lambda_V \sum_i \xi_i c_i^\dagger c_i,\\ H_{\mathrm{SO}} &= i\lambda_{\mathrm{SO}}\sum_{\langle\langle i,j\rangle\rangle}(\nu_{ij}c_i^\dagger s^z c_j + \mathrm{H.c.}),\\ \widetilde{H}_R &= -\lambda_R\sum_{\langle i,j\rangle}[c_i^\dagger(\boldsymbol{s}\times\hat{\boldsymbol{d}}_{ij})_z c_j + \mathrm{H.c.}].\end{aligned} \tag{109}$$

The first term H_K in (108) is the nearest-neighbor hopping. The second term H_V are sublattice potentials with $\xi_i = +1\,(-1)$ for closed (open) circles in Fig. 10. The third term H_{SO} represents the next-nearest-neighbor spin-orbit interaction preserving the z component S_z of the spin, with $\nu_{ij} = \pm 1$ (see Fig. 11). The last term $\widetilde{H}_R$ is the *imaginary* Rashba term, which gives rise to non-Hermiticity. Here, $\hat{\boldsymbol{d}} = \hat{\boldsymbol{y}}$, $\hat{\boldsymbol{d}}_1 = -\frac{\sqrt{3}}{2}\hat{\boldsymbol{x}} - \frac{1}{2}\hat{\boldsymbol{y}}$, and $\hat{\boldsymbol{d}}_2 = +\frac{\sqrt{3}}{2}\hat{\boldsymbol{x}} - \frac{1}{2}\hat{\boldsymbol{y}}$ are illustrated in Fig. 12.

The *imaginary* Rashba term $\widetilde{H}_R$ gives asymmetric nearest-neighbor hopping integrals. The term $\widetilde{H}_R$ is explicitly written as

$$\begin{aligned}\widetilde{H}_R &= -\lambda_R\sum_{\langle i,j\rangle}[c_i^\dagger(\boldsymbol{s}\times\hat{\boldsymbol{d}}_{ij})_z c_j + \mathrm{H.c.}]\\ &= \lambda_R\sum_{i\bullet}[-c_{i+\boldsymbol{d}}^\dagger\sigma_x c_i + c_{i+\boldsymbol{d}_1}^\dagger U_1 c_i + c_{i+\boldsymbol{d}_2}^\dagger U_2 c_i]\\ &\quad -\lambda_R\sum_{i\circ}[-c_{i-\boldsymbol{d}}^\dagger\sigma_x c_i + c_{i-\boldsymbol{d}_1}^\dagger U_1 c_i + c_{i-\boldsymbol{d}_2}^\dagger U_2 c_i],\end{aligned} \tag{110}$$

where $\sum_{i\bullet}$ ($\sum_{i\circ}$) denotes the summation over closed (open) circles in Fig. 10, $U_1 \equiv \frac{1}{2}\sigma_x - \frac{\sqrt{3}}{2}\sigma_y$, and $U_2 \equiv \frac{1}{2}\sigma_x + \frac{\sqrt{3}}{2}\sigma_y$. The hopping integrals are asymmetric for each bond as illustrated in Fig. 13. Let us, respectively, denote two eigenstates of σ_x, U_1, and U_2 as $|\pm\rangle_x$, $|\pm\rangle_1$, and $|\pm\rangle_2$:

$$\sigma_x|\pm\rangle_x = \pm|\pm\rangle_x, \quad U_1|\pm\rangle_1 = \pm|\pm\rangle_1, \quad U_2|\pm\rangle_2 = \pm|\pm\rangle_2. \tag{111}$$

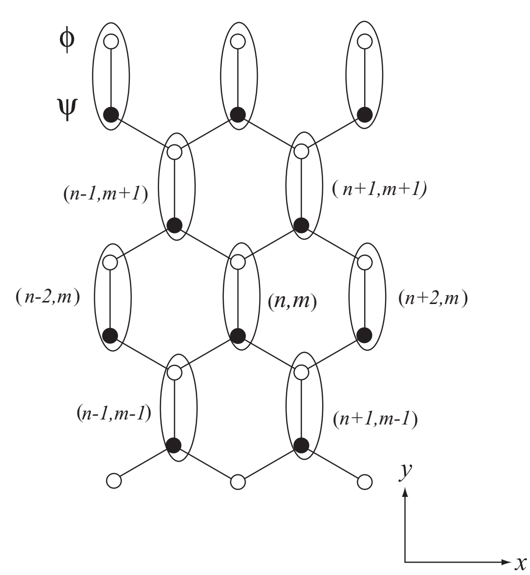

FIG. 10. The honeycomb lattice.

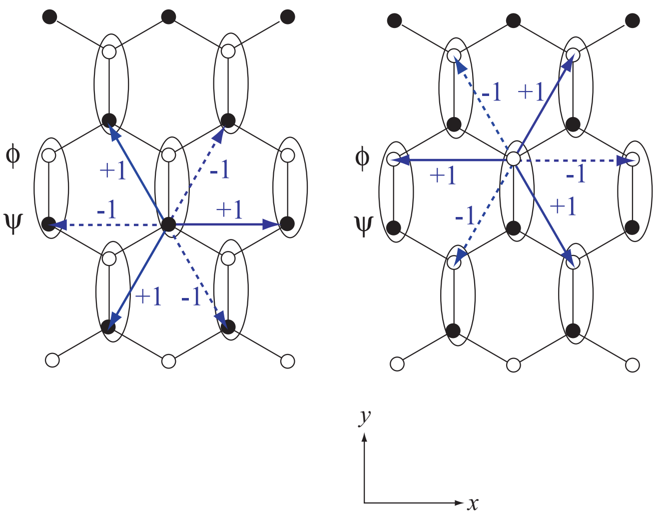

FIG. 11. (Color online) The sign of ν_{ij}.

They are explicitly given by

$$|\pm\rangle_x = \frac{1}{\sqrt{2}}\begin{pmatrix}1\\ \pm 1\end{pmatrix}, \quad |\pm\rangle_1 = \frac{1}{\sqrt{2}}\begin{pmatrix}e^{i\pi/3}\\ \pm 1\end{pmatrix}, \quad |\pm\rangle_2 = \frac{1}{\sqrt{2}}\begin{pmatrix}e^{-i\pi/3}\\ \pm 1\end{pmatrix}. \tag{112}$$

For each eigenstate, the hopping integrals $t+\lambda_R\sigma_x$, $t+\lambda_R U_1$, and $t+\lambda_R U_2$ read as

$$(t+\lambda_R\sigma_x)|\pm\rangle_x = (t\pm\lambda_R)|\pm\rangle_x, \quad (t+\lambda_R U_{1(2)})|\pm\rangle_{1(2)} = (t\pm\lambda_R)|\pm\rangle_{1(2)}, \tag{113}$$

and the hopping integrals $t-\lambda_R\sigma_x$, $t-\lambda_R U_1$, and $t-\lambda_R U_2$ yield

$$(t-\lambda_R\sigma_x)|\pm\rangle_x = (t\mp\lambda_R)|\pm\rangle_x, \quad (t-\lambda_R U_{1(2)})|\pm\rangle_{1(2)} = (t\mp\lambda_R)|\pm\rangle_{1(2)}. \tag{114}$$

The sign difference between (113) and (114) implies that the hopping integrals [for the basis $(|\pm\rangle_x, |\pm\rangle_1, |\pm\rangle_2)$] along the bonds parallel to $(\boldsymbol{d}, \boldsymbol{d}_1, \boldsymbol{d}_2)$ are asymmetric: $(t+\lambda_R)$ in one direction and $(t-\lambda_R)$ in the other.

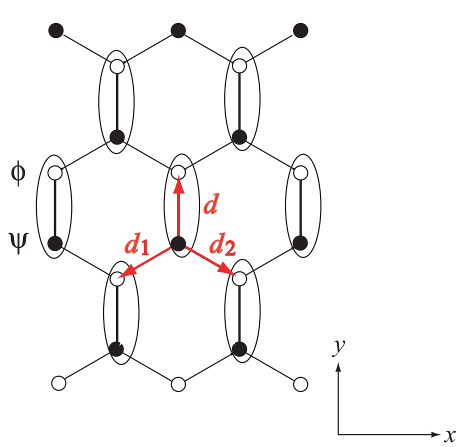

FIG. 12. (Color online) $\boldsymbol{d}$, $\boldsymbol{d}_1$, and $\boldsymbol{d}_2$.

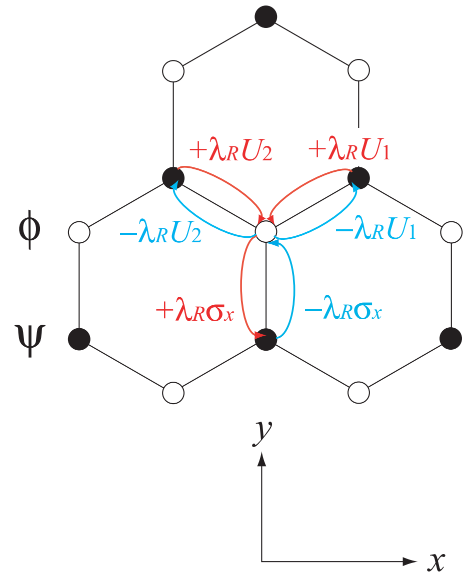

FIG. 13. (Color online) The nearest-neighbor hopping integrals of *imaginary* Rashba terms. The hopping integrals of each bond are asymmetric. [$U_1 = \frac{1}{2}\sigma_x - \frac{\sqrt{3}}{2}\sigma_y$ and $U_2 = \frac{1}{2}\sigma_x + \frac{\sqrt{3}}{2}\sigma_y$.]

We also note that the *imaginary* Rashba spin-orbit interaction can be regarded as an *imaginary* SU(2) gauge potential (see the Appendix). In this sense, our model can be regarded as a non-Abelian generalization of the Hatano-Nelson model in which an *imaginary* U(1) vector potential[23–25] was considered.

Now, we consider the Hamiltonian in the momentum space. By performing the Fourier transformation with respect to (n,m) in Fig. 10, the Hamiltonian in the momentum space is obtained as

$$H(\boldsymbol{k}) = \sum_{a=1,2} d_a(\boldsymbol{k})\tilde{\Gamma}_a + \sum_{ab=12,15} d_{ab}(\boldsymbol{k})\tilde{\Gamma}_{ab} + i\sum_{a=3,4} d_a(\boldsymbol{k})\tilde{\Gamma}_a + i\sum_{ab=23,24} d_{ab}(\boldsymbol{k})\tilde{\Gamma}_{ab}, \tag{115}$$

where $\tilde{\Gamma}_{ab} = [\tilde{\Gamma}_a, \tilde{\Gamma}_b]/(2i)$, and

$$\begin{aligned} d_1 &= t(1+2\cos x\cos y), \quad d_2 = \lambda_V, \\ d_3 &= \lambda_R(1-\cos x\cos y), \quad d_4 = -\sqrt{3}\lambda_R\sin x\sin y, \\ d_{12} &= -2t\cos x\sin y, \\ d_{15} &= \lambda_{\rm SO}(2\sin 2x - 4\sin x\cos y), \\ d_{23} &= -\lambda_R\cos x\sin y, \quad d_{24} = \sqrt{3}\lambda_R\sin x\cos y, \end{aligned} \tag{116}$$

with $x = k_x a/2$ and $y = \sqrt{3}k_y a/2$. Here, we have adopted the following gamma matrices:

$$\tilde{\Gamma}_{(1,2,3,4,5)} = (\sigma^x\otimes I, \sigma^z\otimes I, \sigma^y\otimes\sigma^x, \sigma^y\otimes\sigma^y, \sigma^y\otimes\sigma^z). \tag{117}$$

The Hamiltonian (115) possesses the pseudo-Hermiticity

$$\eta H(\boldsymbol{k})^\dagger\eta^{-1} = H(\boldsymbol{k}), \quad \eta = i\tilde{\Gamma}_4\tilde{\Gamma}_3 \tag{118}$$

and time-reversal invariance with $\widetilde{\Theta}_+^2 = +1$:

$$\widetilde{\Theta}_+ H(-\boldsymbol{k})\widetilde{\Theta}_+^{-1} = H(\boldsymbol{k}), \quad \widetilde{\Theta}_+ = i\widetilde{\Gamma}_5\widetilde{\Gamma}_4 \cdot K. \qquad (119)$$

These symmetries are simply understood by noticing that the Hamiltonian (115) is a special case of (62) by identifying $(\widetilde{\Gamma}_1,\widetilde{\Gamma}_2,\widetilde{\Gamma}_3,\widetilde{\Gamma}_4,\widetilde{\Gamma}_5)$ in Eq. (117) with $(\Gamma_3,\Gamma_5,\Gamma_2,\Gamma_1,\Gamma_4)$ in Eq. (54). From the anticommutation relation $\{\eta,\widetilde{\Theta}_+\} = 0$, the time-reversal-invariant Chern number $C_{\rm TRI}$ can be introduced in a manner similar to the previous sections. In the following, by using the time-reversal-invariant Chern number, we argue the topological stability of the edge states of the Hamiltonian (108) with zigzag edges (Fig. 2).

First, we discuss the Hermitian case $\lambda_R = 0$.[7,15] For $\lambda_R = 0$, in addition to the time-reversal symmetry $\widetilde{\Theta}_+$ with $\widetilde{\Theta}_+^2 = +1$ [Eq. (119)], the Hamiltonian (115) has another time-reversal symmetry $\widetilde{\Theta}_-$ with $\widetilde{\Theta}_-^2 = -1$:

$$\widetilde{\Theta}_- H(-\boldsymbol{k})\widetilde{\Theta}_-^{-1} = H(\boldsymbol{k}), \quad \widetilde{\Theta}_- = \widetilde{\Gamma}_3\widetilde{\Gamma}_5 \cdot K. \qquad (120)$$

Moreover, for $\lambda_R = 0$, the pseudo-Hermiticity (118) reduces to

$$[H(\boldsymbol{k}),\eta] = 0. \qquad (121)$$

Thus, the metric operator η becomes a conserved quantity, the eigenvalue of which is either $+1$ or -1. By regarding η as the z component of the spin, the spin Chern number C_s can be defined.[12] For $\lambda_V < 3\sqrt{3}\lambda_{\rm SO}$, where the spin Chern number is nonzero, i.e., $C_s = 1$, gapless edge modes appear as shown in Fig. 14(a). On the other hand, for $\lambda_V > 3\sqrt{3}\lambda_{\rm SO}$, the system is in the topologically trivial insulating phase with $C_s = 0$. In this phase, gapless edge modes do not appear as illustrated in Fig. 14(b).

Now, we include the non-Hermitian term λ_R. Once the non-Hermitian term is nonzero, η is no longer conserved, thus, the spin Chern number C_s is not well defined. By using the time-reversal-invariant Chern number $C_{\rm TRI}$, however, we can argue the topological stability of the gapless edge modes. Let us first consider the region $\lambda_V < 3\sqrt{3}\lambda_{\rm SO}$ as shown in Figs. 15 and 16. When λ_R is small, the gapless edge modes that appear in the Hermitian case ($\lambda_R = 0$) still remain [Figs. 15(a) and 15(b)]. These gapless edge states are topologically protected by the time-reversal-invariant Chern number $C_{\rm TRI} = 1$: For small λ_R, the non-Hermitian Hamiltonian (115) can be adiabatically deformed into the Hermitian one ($\lambda_R = 0$) without closing the bulk gap, and the time-reversal-invariant Chern number $C_{\rm TRI}$ reduces to the spin Chern number C_s in the Hermitian limit. Thus, from the adiabatic continuity, we have $C_{\rm TRI} = C_s = 1$. On the other hand, for sufficiently large λ_R, the bulk gap closes and $C_{\rm TRI}$ becomes ill defined. Correspondingly, the gapless edge modes disappear.

Next, consider the region $\lambda_V > 3\sqrt{3}\lambda_{\rm SO}$. In the presence of weak non-Hermiticity λ_R, gapless edge modes do not appear [Figs. 17(a) and 18(a)]. This is because the bulk gap has not yet closed and the system remains a topologically trivial phase with $C_{\rm TRI} = 0$. If we further increase λ_R, the bulk gap closes near $ak_x \sim 2\pi/3$ and $4\pi/3$ at a critical value of λ_R, then the bulk gap opens again [Figs. 17(b) and 18(b).] In this region of λ_R, gapless edge modes appear that are topologically protected by the time-reversal-invariant Chern number. For sufficiently large λ_R, the bulk gap closes once again at $ak_x \sim \pi$, and the edge modes disappear as shown in Figs. 17(c) and 18(c).

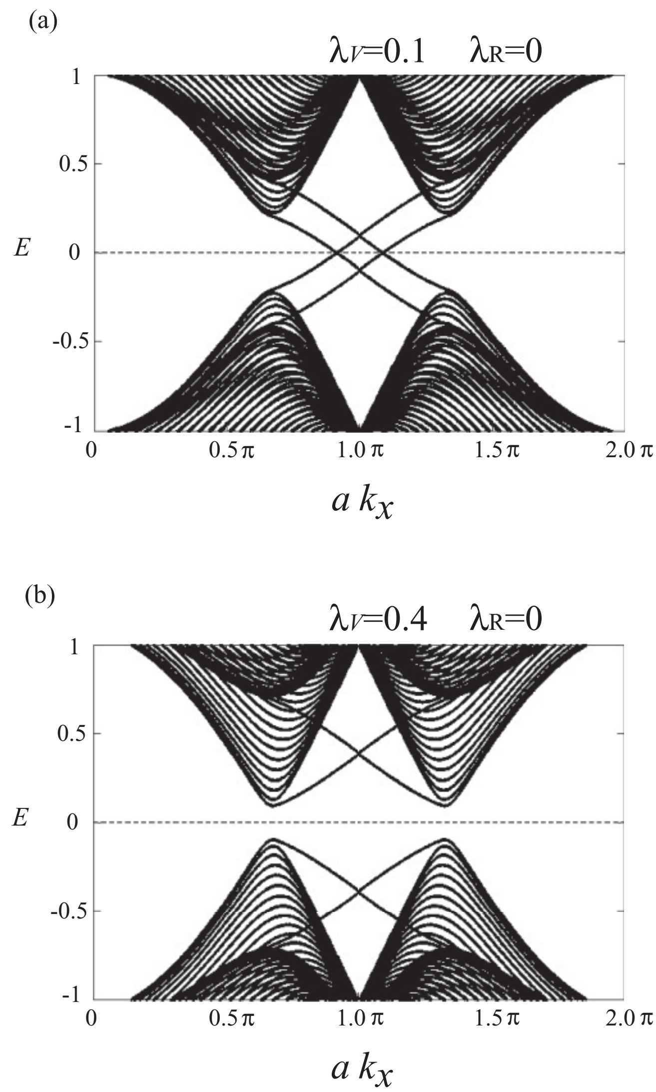

FIG. 14. (Color online) The energy bands of the Kane-Mele model (108) with zigzag edges along the x direction for $t = 1.0$, $\lambda_{\rm SO} = 0.06$, $\lambda_R = 0$ (Hermitian case), and (a) $\lambda_V = 0.1$, (b) $\lambda_V = 0.4$. Here, a is the lattice constant and k_x the momentum in the x direction. In (a), a gapless helical edge state appears on each edge, while in (b), no gapless edge state is obtained.

VI. SUMMARY AND DISCUSSION

In this work, we investigated edge modes and their topological stability in non-Hermitian models. We analyzed three types of models: SU(1,1) lattice model realized on graphene with pure imaginary sublattice potential, SO(3,2) Luttinger model on 2D square lattice, and SO(3,2) Kane-Mele model with asymmetric hopping integrals on graphene. The energy spectra of such non-Hermitian models generally contain complex eigenvalues. In this paper, we focused on the real parts of the edge bands and characterized them by using topological arguments. (The imaginary part of eigenvalues brings decay of wave function with time.) For the SU(1,1) lattice model,

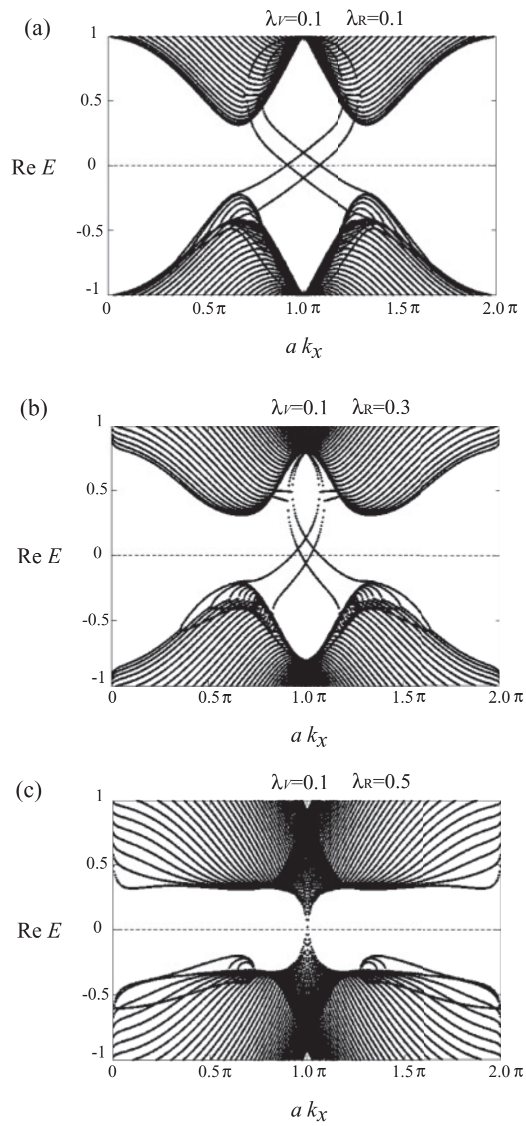

FIG. 15. (Color online) The real part of the energy bands of the non-Hermitian Kane-Mele model (108) with zigzag edge along the x direction. We plot the results for $t = 1.0$, $\lambda_{\rm SO} = 0.06$, $\lambda_V = 0.1$, and various values of non-Hermitian parameter λ_R. Here, a is the lattice constant and k_x is the momentum in the x direction. In (a) and (b), we have gapless edge states. In (c), the bulk gap closes, and no gapless edge state exists.

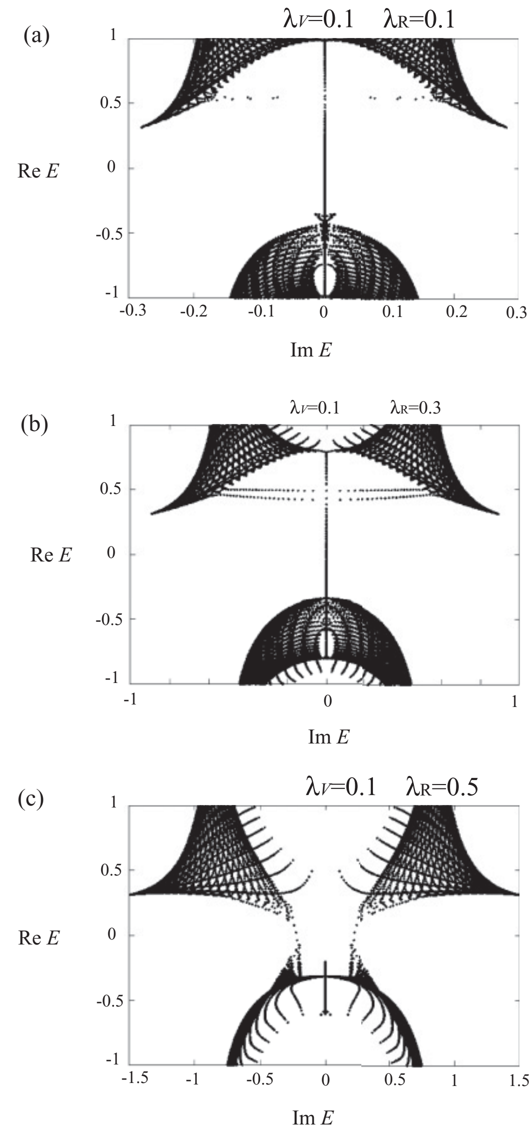

FIG. 16. The real vs imaginary part of the energy bands of non-Hermitian Kane-Mele model (108) with zigzag edges along the x direction. We plot the results for $t = 1.0$, $\lambda_{\rm SO} = 0.06$, $\lambda_V = 0.1$, and various values of the non-Hermitian parameter λ_R. The data (a) and (b) indicate that the energy of the gapless edge states [Figs. 15(a) and 15(b)] is real. On the other hand, the bulk state supports the imaginary part of the energy.

with numerical calculations, we found that the edge states with $\mathrm{Re}E = 0$ are robust against small non-Hermitian perturbation. We gave topological arguments for the robustness of edge state. Meanwhile, the SO(3,2) Luttinger and the SO(3,2) Kane-Mele models are time-reversal-invariant non-Hermitian models with $\Theta^2 = +1$. The generalized Kramers theorem suggests the existence of helical edge modes in the models. The numerical calculations indeed confirmed the existence of helical edge modes and robustness of them under the small non-Hermitian perturbations. We introduced time-reversal-invariant Chern number inherent to non-Hermitian models, and gave topological arguments about the stability of helical edge modes.

In this paper, we adopted non-Hermitian models, the Hermitian counterparts of which are typical topological insulators in 2D. There are many types of topological insulators, such as topological superconductors, 3D topological insulators, etc. It would be interesting to consider non-Hermitian generalizations of these various topological insulators, where gapless edge modes could also appear. The topological arguments for non-Hermitian systems presented in this paper would constitute the first step to introducing topological invariants characterizing gapless edge modes of other non-Hermitian models.

Note added. Recently, we noticed Ref. 43 in which the SU(1,1) and SO(3,2) models are discussed in the context of topological insulators. Their numerical calculations of the lattice version of the SU(1,1) coincide with our results. In

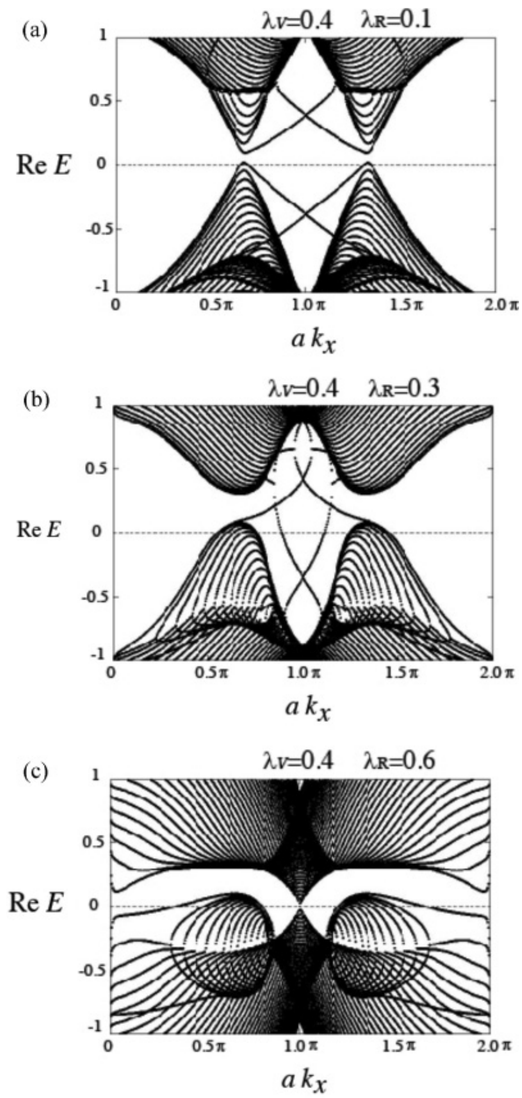

FIG. 17. (Color online) The real part of the energy bands of the non-Hermitian Kane-Mele model (108) with zigzag edge along the x direction. We plot the results for $t = 1.0$, $\lambda_{\rm SO} = 0.06$, $\lambda_V = 0.4$, and various values of non-Hermitian parameter λ_R. Here, a is the lattice constant and k_x is the momentum in the x direction. In (a), no gapless edge state exists, while in (b), topologically protected gapless edge states appear. In (c), the bulk gap closes and the topologically protected gapless edge states disappear.

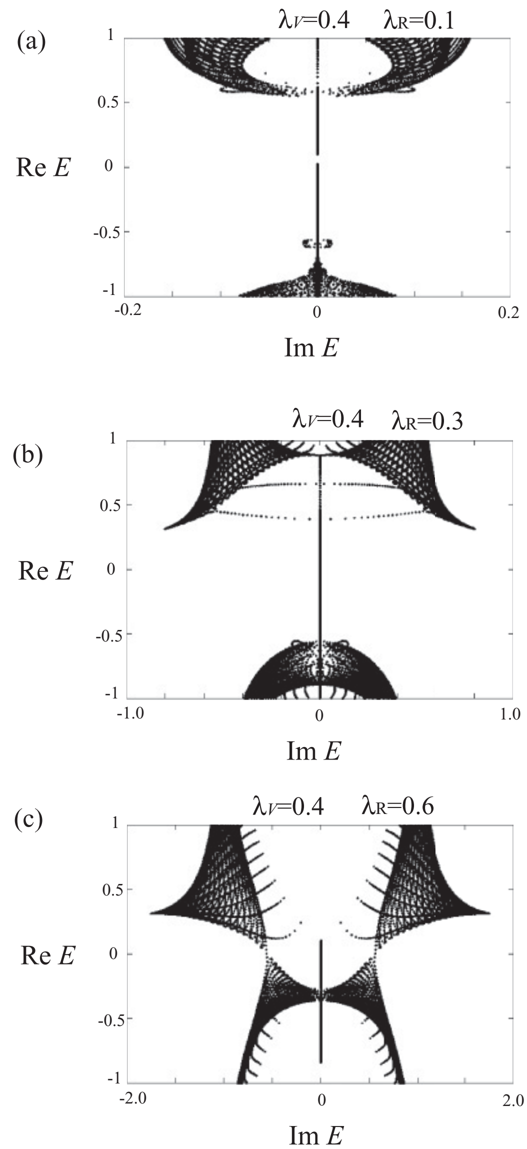

FIG. 18. The real vs imaginary part of the energy bands of non-Hermitian Kane-Mele model (108) with zigzag edges along the x direction. We plot the results for $t = 1.0$, $\lambda_{\rm SO} = 0.06$, $\lambda_V = 0.4$, and various values of the non-Hermitian parameter λ_R. The data (b) indicate that the energy of the gapless edge states [Fig. 17(b)] is real. On the other hand, the bulk state supports the imaginary part of the energy.

Ref. 43, the authors concluded that the appearance of the complex eigenvalues is an indication of the nonexistence of the topological insulator phase in non-Hermitian models. In this paper, we focused on the real part of the complex eigenvalues and explored the robustness of the gapless edge modes on the basis of topological stability arguments. The "topological phase" in this paper is referred to the phase in which the real part of edge modes is stable under small non-Hermitian perturbations.

ACKNOWLEDGMENTS

We acknowledge the ISSP visiting program that enabled the collaboration. K.E. was supported in part by Global COE Program "the Physical Sciences Frontier," MEXT, Japan. This work was supported in part by a Grant-in Aid for Scientific Research from MEXT of Japan, Grants No. 22103005 (Innovative Areas "Topological Quantum Phenomena"), No. 22540383, and No. 23740212.

APPENDIX: IMAGINARY RASHBA INTERACTIONS AND IMAGINARY SU(2) GAUGE POTENTIALS

Let us first consider continuum Hamiltonians with *imaginary* Rashba couplings $i\lambda$ (λ: real constants):

$$\begin{aligned} H &= \frac{1}{2m}\left(p_x^2 + p_y^2\right) + i\lambda(p_x\sigma_y - p_y\sigma_x) \\ &= \frac{1}{2m}(p_x + i\theta\sigma_y)^2 + \frac{1}{2m}(p_y - i\theta\sigma_x)^2 + m\lambda^2, \qquad \text{(A1)} \end{aligned}$$

where $\theta \equiv m\lambda$. From (A1), we find that the *imaginary* Rashba interaction can be regarded as an *imaginary* SU(2) gauge potential

$$(\widetilde{A}_x,\widetilde{A}_y) = (-i\theta\sigma_y, i\theta\sigma_x). \tag{A2}$$

This *imaginary* gauge potential acquires *scale transformations* $\widetilde{U}_x$ and $\widetilde{U}_y$ when we proceed by a unit length along the x and y directions, respectively:

$$\widetilde{U}_x = e^{\theta\sigma_y}, \quad \widetilde{U}_y = e^{-\theta\sigma_x}. \tag{A3}$$

Now, we perform scale transformations $H' = \widetilde{U}(x,y)^{-1}H\widetilde{U}(x,y)$ with

$$\widetilde{U}(x,y) = e^{\theta\sigma_y x}e^{-\theta\sigma_x y}. \tag{A4}$$

For the first term of the Hamiltonian (A1), we have

$$\begin{aligned}
&\widetilde{U}(x,y)^{-1}(p_x + i\theta\sigma_y)^2\widetilde{U}(x,y)\\
&= e^{\theta\sigma_x y}e^{-\theta\sigma_y x}\left(-i\frac{\partial}{\partial x} + i\theta\sigma_y\right)^2 e^{\theta\sigma_y x}e^{-\theta\sigma_x y}\\
&= -e^{\theta\sigma_x y}\frac{\partial^2}{\partial x^2}e^{-\theta\sigma_x y} = p_x^2.
\end{aligned} \tag{A5}$$

For the second term of the Hamiltonian (A1), we have

$$\begin{aligned}
&\widetilde{U}(x,y)^{-1}(p_y - i\theta\sigma_x)^2\widetilde{U}(x,y)\\
&= e^{\theta\sigma_x y}e^{-\theta\sigma_y x}(p_y - i\theta\sigma_x)^2 e^{\theta\sigma_y x}e^{-\theta\sigma_x y}\\
&= e^{-2i\theta^2 xy\sigma_z}e^{-\theta\sigma_y x}e^{\theta\sigma_x y}\left(-i\frac{\partial}{\partial y} - i\theta\sigma_x\right)^2\\
&\quad\times e^{-\theta\sigma_x y}e^{\theta\sigma_y x}e^{2i\theta^2 xy\sigma_z}\\
&= -e^{-2i\theta^2 xy\sigma_z}e^{-\theta\sigma_y x}\frac{\partial^2}{\partial y^2}e^{\theta\sigma_y x}e^{2i\theta^2 xy\sigma_z}\\
&= -e^{-2i\theta^2 xy\sigma_z}\frac{\partial^2}{\partial y^2}e^{2i\theta^2 xy\sigma_z} = -\left(\frac{\partial}{\partial y} + 2i\theta^2\sigma_z x\right)^2\\
&= (p_y + 2\theta^2\sigma_z x)^2,
\end{aligned} \tag{A6}$$

where we used the Baker-Campbell-Hausdorff formula up to the leading order of θ. Therefore, we have

$$H' = \frac{1}{2m}p_x^2 + \frac{1}{2m}(p_y + 2\theta^2\sigma_z x)^2 + m\lambda^2. \tag{A7}$$

The Hamiltonian (A7) is Hermitian and coincides with the one with *real* Rashba coupling λ (under the transformation $\sigma_z \to -\sigma_z$). We recall that Rashba interactions with *real* couplings λ can be regarded as SU(2) gauge potentials[44]

$$(A_x, A_y) = (-\theta\sigma_y, \theta\sigma_x), \tag{A8}$$

which give field strengths

$$\begin{aligned}
F_{xy} &= \partial_x A_y - \partial_y A_x - i[A_x, A_y]\\
&= i\theta^2[\sigma_y,\sigma_x] = 2\theta^2\sigma_z.
\end{aligned} \tag{A9}$$

Actually, Eq. (A7) with $\sigma_z \to -\sigma_z$ gives field strengths $F_{xy} = 2\theta^2\sigma_z$ [Eq. (A9)].

Although non-Hermitian Hamiltonian H is transformed into Hermitian Hamiltonian H' by the scale transformations $\widetilde{U}(x,y)$, non-Hermiticity affects the boundary conditions. Suppose that right eigenfunctions $\psi^R(x,y)$ and left eigenfunctions $\psi^L(x,y)$ of H have periodic boundary conditions both in x and the y directions:

$$\begin{aligned}
\psi^R(L_x,y) = \psi^R(0,y), \quad \psi^L(L_x,y) = \psi^L(0,y),\\
\psi^R(x,L_y) = \psi^R(x,0), \quad \psi^L(x,L_y) = \psi^L(x,0).
\end{aligned} \tag{A10}$$

From the boundary condition in the x direction, eigenfunctions $\psi'(x,y) = \widetilde{U}(x,y)^{-1}\psi^R(x,y)$ of H' are found to satisfy

$$\begin{aligned}
\psi'(L_x,y) &= \widetilde{U}(L_x,y)^{-1}\psi^R(L_x,y)\\
&= \widetilde{U}(L_x,y)^{-1}\widetilde{U}(0,y)\widetilde{U}(0,y)^{-1}\psi^R(0,y)\\
&= e^{\theta\sigma_x y}e^{-\theta\sigma_y L_x}e^{-\theta\sigma_x y}\psi'(0,y)\\
&= e^{-\theta\sigma_y L_x}e^{-2i\theta^2\sigma_z L_x y}\psi'(0,y)
\end{aligned} \tag{A11}$$

and

$$\psi'(L_x,y)^\dagger = \psi'(0,y)^\dagger e^{2i\theta^2\sigma_z L_x y}e^{\theta\sigma_y L_x}. \tag{A12}$$

Similarly, the boundary condition in the y direction gives

$$\psi'(x,L_y) = e^{\theta\sigma_x L_y}\psi'(x,0), \quad \psi'(x,L_y)^\dagger = \psi'(x,0)^\dagger e^{-\theta\sigma_x L_y}. \tag{A13}$$

Let us now generalize the above arguments to lattice systems. For simplicity, we consider a tight-binding model on the square lattice with the nearest-neighbor hopping integrals with *imaginary* SU(2) gauge fields:

$$\begin{aligned}
H = &\sum_{(n,m)}[c_{(n+1,m)}^\dagger e^{\theta\sigma_y}c_{(n,m)} + c_{(n-1,m)}^\dagger e^{-\theta\sigma_y}c_{(n,m)}\\
&+ c_{(n,m+1)}^\dagger e^{-\theta\sigma_x}c_{(n,m)} + c_{(n,m-1)}^\dagger e^{\theta\sigma_x}c_{(n,m)}]\\
&+ \sum_{(n,m)}[c_{(n,m)}^\dagger e^{-\theta\sigma_y}c_{(n+1,m)} + c_{(n,m)}^\dagger e^{\theta\sigma_y}c_{(n-1,m)}\\
&+ c_{(n,m)}^\dagger e^{\theta\sigma_x}c_{(n,m+1)} + c_{(n,m)}^\dagger e^{-\theta\sigma_x}c_{(n,m-1)}],
\end{aligned} \tag{A14}$$

which is illustrated in Fig. 19. By scale transformations

$$c_{(n,m)} = e^{\theta\sigma_y n}e^{-\theta\sigma_x m}\widetilde{c}_{(n,m)}, \quad c_{(n,m)}^\dagger = \widetilde{c}_{(n,m)}^\dagger e^{\theta\sigma_x m}e^{-\theta\sigma_y n}, \tag{A15}$$

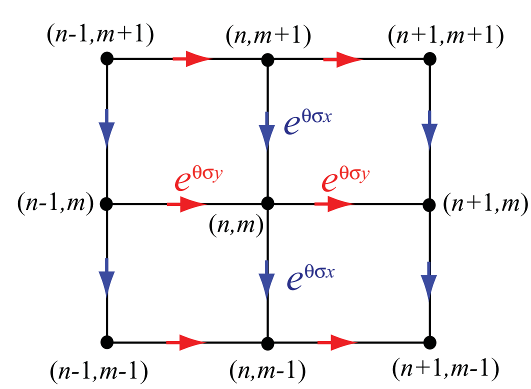

FIG. 19. (Color online) Tight-binding model on the square lattice with *imaginary* SU(2) gauge fields.

the Hamiltonian (A14) is transformed into

$$\begin{aligned} H' = \sum_{(n,m)} [&\widetilde{c}^{\dagger}_{(n+1,m)}\widetilde{c}_{(n,m)} + \widetilde{c}^{\dagger}_{(n-1,m)}\widetilde{c}_{(n,m)} \\ &+ \widetilde{c}^{\dagger}_{(n,m+1)} e^{-2i\theta^2\sigma_z n}\widetilde{c}_{(n,m)} + \widetilde{c}^{\dagger}_{(n,m-1)} e^{2i\theta^2\sigma_z n}\widetilde{c}_{(n,m)}] \\ &+ \sum_{(n,m)} [\widetilde{c}^{\dagger}_{(n,m)}\widetilde{c}_{(n+1,m)} + \widetilde{c}^{\dagger}_{(n,m)}\widetilde{c}_{(n-1,m)} \\ &+ \widetilde{c}^{\dagger}_{(n,m)} e^{2i\theta^2\sigma_z n}\widetilde{c}_{(n,m+1)} + \widetilde{c}^{\dagger}_{(n,m)} e^{-2i\theta^2\sigma_z n}\widetilde{c}_{(n,m-1)}], \end{aligned} \tag{A16}$$

where we used the Baker-Campbell-Hausdorff formula up to the leading order of θ. The Hamiltonian (A16) is the tight-binding model with SU(2) gauge fields, which gives an observable flux $2\theta^2\sigma_z$ per plaquette (under a transformation $\sigma_z \to -\sigma_z$).

Let us impose the periodic boundary condition on the original Hamiltonian H [Eq. (A14)]:

$$\begin{aligned} c_{(L_x,m)} &= c_{(0,m)}, \quad c^{\dagger}_{(L_x,m)} = c^{\dagger}_{(0,m)}, \\ c_{(n,L_y)} &= c_{(n,0)}, \quad c^{\dagger}_{(n,L_y)} = c^{\dagger}_{(n,0)}. \end{aligned} \tag{A17}$$

Then, non-Hermiticity appears as boundary conditions for the Hamiltonian H' [Eq. (A16)]:

$$\begin{aligned} \widetilde{c}_{(L_x,m)} &= e^{-\theta\sigma_y L_x} e^{-2i\theta^2\sigma_z L_x m}\widetilde{c}_{(0,m)}, \\ \widetilde{c}^{\dagger}_{(L_x,m)} &= \widetilde{c}^{\dagger}_{(0,m)} e^{2i\theta^2\sigma_z L_x m} e^{\theta\sigma_y L_x}, \\ \widetilde{c}_{(n,L_y)} &= e^{\theta\sigma_x L_y}\widetilde{c}_{(n,0)}, \\ \widetilde{c}^{\dagger}_{(n,L_y)} &= \widetilde{c}^{\dagger}_{(n,0)} e^{-\theta\sigma_x L_y}. \end{aligned} \tag{A18}$$

[1] S. Murakami, N. Nagaosa, and S.-C. Zhang, Science **301**, 1348 (2003).
[2] S. Murakami, N. Nagaosa, and S.-C. Zhang, Phys. Rev. B **69**, 235206 (2004).
[3] J. M. Luttinger, Phys. Rev. **102**, 1030 (1956).
[4] Y. K. Kato, R. C. Myers, A. C. Gossard, and D. D. Awschalom, Science **306**, 1910 (2004).
[5] J. Wunderlich, B. Kaestner, J. Sinova, and T. Jungwirth, Phys. Rev. Lett. **94**, 047204 (2005).
[6] S. Murakami, N. Nagaosa, and S.-C. Zhang, Phys. Rev. Lett. **93**, 156804 (2004).
[7] C. L. Kane and E. J. Mele, Phys. Rev. Lett. **95**, 226801 (2005).
[8] B. A. Bernevig and S.-C. Zhang, Phys. Rev. Lett. **96**, 106802 (2006).
[9] M. König, S. Wiedmann, C. Brüne, A. Roth, H. Buhmann, L. W. Molenkamp, X.-L. Qi, and S.-C. Zhang, Science **318**, 766 (2007).
[10] B. A. Bernevig, T. L. Hughes, and S.-C. Zhang, Science **314**, 1757 (2006).
[11] X.-L. Qi, Y.-S. Wu, and S.-C. Zhang, Phys. Rev. B **74**, 085308 (2006).
[12] D. N. Sheng, Z. Y. Weng, L. Sheng, and F. D. M. Haldane, Phys. Rev. Lett. **97**, 036808 (2006).
[13] D. J. Thouless, M. Kohmoto, M. P. Nightingale, and M. den Nijs, Phys. Rev. Lett. **49**, 405 (1982).
[14] M. Kohmoto, Ann. Phys. (NY) **160**, 343 (1985).
[15] C. L. Kane and E. J. Mele, Phys. Rev. Lett. **95**, 146802 (2005).
[16] C. Wu, B. A. Bernevig, and S.-C. Zhang, Phys. Rev. Lett. **96**, 106401 (2006).
[17] M. Sato, K. Hasebe, K. Esaki, and M. Kohmoto, e-print arXiv:1106.1806.
[18] K. Hasebe, Phys. Rev. D **81**, 041702(R) (2010).
[19] K. Hasebe, J. Math. Phys. **51**, 053524 (2010).
[20] D. C. Brody and E.-M. Graefe, J. Phys. A: Math. Gen. **44**, 072001 (2011).
[21] D. C. Brody and E.-M. Graefe, e-print arXiv:1105.3604.
[22] D. C. Brody and E.-M. Graefe, Acta Polytech. **51**, 14 (2011).
[23] N. Hatano and D. R. Nelson, Phys. Rev. Lett. **77**, 570 (1996).
[24] N. Hatano and D. R. Nelson, Phys. Rev. B **56**, 8651 (1997).
[25] N. Hatano and D. R. Nelson, Phys. Rev. B **58**, 8384 (1998).
[26] S.-L. Zhu, B. Wang, and L.-M. Duan, Phys. Rev. Lett. **98**, 260402 (2007).
[27] Y. B.-Aryeh, A. Mann, and I. Yaakov, J. Phys. A: Math. Gen. **37**, 12059 (2004).
[28] M. S. Rudner and L. S. Levitov, Phys. Rev. Lett. **102**, 065703 (2009).
[29] M. S. Rudner and L. S. Levitov, Phys. Rev. B **82**, 155418 (2010).
[30] M. Fujita, K. Wakabayashi, K. Nakada, and K. Kusakabe, J. Phys. Soc. Jpn. **65**, 1920 (1996).
[31] J. E. Avron, R. Seiler, and B. Simon, Phys. Rev. Lett. **51**, 51 (1983).
[32] A. P. Schnyder, S. Ryu, A. Furusaki, and A. W. W. Ludwig, Phys. Rev. B **78**, 195125 (2008).
[33] M. Sato, Y. Tanaka, K. Yada, and T. Yokoyama, Phys. Rev. B **83**, 224511 (2011).
[34] A. Mostafazadeh, J. Math. Phys. **43**, 205 (2002); **43**, 2814 (2002); **43**, 3944 (2002).
[35] A. Mostafazadeh, Int. J. Geom. Meth. Mod. Phys. **7**, 1191 (2010).
[36] D. Bernard and A. LeClair, e-print arXiv:cond-mat/0110649.
[37] Note that the representation of the gamma matrices in this paper is different from the one we used in Ref. 17. Our results are independent of the representation we choose since these representations are unitary equivalent to each other.
[38] C. M. Bender and S. Boettcher, Phys. Rev. Lett. **80**, 5243 (1998).
[39] C. M. Bender, S. Boettcher, and P. N. Meisinger, J. Math. Phys. **40**, 2201 (1999).
[40] C. M. Bender, Rep. Prog. Phys. **70**, 947 (2007).
[41] The model (67) with $d_1 = d_2 = 0$ corresponds to the Luttinger Hamiltonian in a symmetric quantum well along the z direction. When the quantum well is narrow enough, we could replace k_z-dependent terms $\cos k_z \sim k_z^2$ with the expectation value $e_s \equiv \langle k_z^2 \rangle$ by eigenstates corresponding to the lowest 2D band (see Ref. 11).
[42] A. I. Nesterov and F. A. de la Cruz, J. Phys. A: Math. Gen. **41**, 485304 (2008).
[43] Y. C. Hu and T. L. Hughes, Phys. Rev. B **84**, 153101 (2011).
[44] N. Hatano, R. Shirasaki, and H. Nakamura, Phys. Rev. A **75**, 032107 (2007).